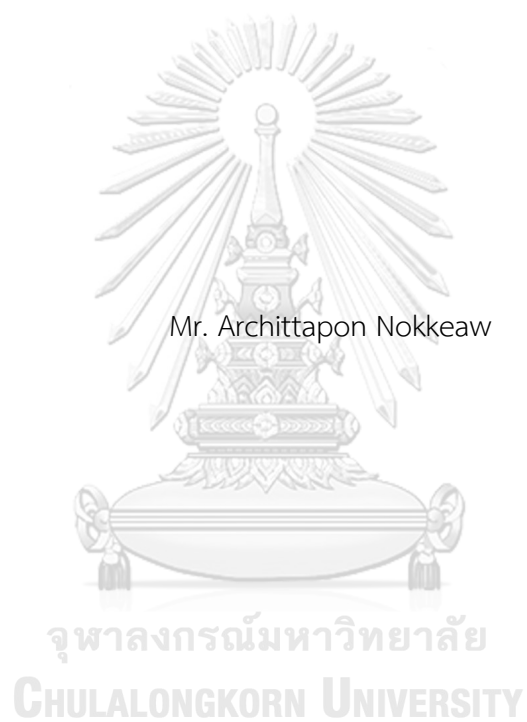


Exploring roles of miR-885-5p in hepatocellular carcinoma



A Thesis Submitted in Partial Fulfillment of the Requirements
for the Degree of Master of Science in Medical Biochemistry

Department of Biochemistry

FACULTY OF MEDICINE

Chulalongkorn University

Academic Year 2022

Copyright of Chulalongkorn University



จุฬาลงกรณ์มหาวิทยาลัย
CHULALONGKORN UNIVERSITY

การศึกษาหน้าที่ของไมโครอาร์เอ็นเอแปดแปดห้าห้าพีในโรคมะเร็งเซลล์ตับ



วิทยานิพนธ์นี้เป็นส่วนหนึ่งของการศึกษาตามหลักสูตรปริญญาวิทยาศาสตรมหาบัณฑิต
สาขาวิชาชีวเคมีทางการแพทย์ ภาควิชาชีวเคมี
คณะแพทยศาสตร์ จุฬาลงกรณ์มหาวิทยาลัย
ปีการศึกษา 2565
ลิขสิทธิ์ของจุฬาลงกรณ์มหาวิทยาลัย

Thesis Title Exploring roles of miR-885-5p in hepatocellular carcinoma

By Mr. Archittapon Nokkeaw

Field of Study Medical Biochemistry

Thesis Advisor CHAIYABOOT ARIYACHET, Ph.D.

Accepted by the FACULTY OF MEDICINE, Chulalongkorn University in Partial Fulfillment of the Requirement for the Master of Science

..... Dean of the FACULTY OF MEDICINE
(Associate Professor CHANCHAI SITTIPUNT, M.D.)

THESIS COMMITTEE

..... Chairman
(Naphat Chantaravisoot, Ph.D.)

..... Thesis Advisor
(CHAIYABOOT ARIYACHET, Ph.D.)

..... Examiner
(PORNCHAI KAEWSAPSAK, Ph.D.)

..... External Examiner
(Assistant Professor Woranop Sukparangsi, Ph.D.)

อชิตพล นกแก้ว : การศึกษาหน้าที่ของไมโครอาร์เอ็นเอแปดแปดห้าห้าพีในโรคมะเร็งเซลล์ตับ. (Exploring roles of miR-885-5p in hepatocellular carcinoma) อ.ที่ปรึกษาหลัก : อ. ดร.ชัย บุตร อริยะเชษฐ

โรคมะเร็งตับเซลล์ตับ หรือ HCC เป็นมะเร็งตับรูปแบบหนึ่งที่พบมากที่สุด โดยส่งผลกระทบต่อประเทศไทยต่อประเทศในภูมิภาคเอเชียตะวันออกเฉียงใต้ ยิ่งไปกว่านั้นโรคมะเร็งเซลล์ตับยังเป็นสาเหตุของการเสียชีวิตจากมะเร็งทั่วโลกเป็นอันดับที่สาม สิ่งเหล่านี้ล้วนเนื่องมาจากอัตราการรอดชีวิตต่ำและอัตราการกลับมาเป็นโรครื้อซ้ำที่สูง ซึ่งมีสาเหตุจากขาดการรักษาที่มีประสิทธิภาพ ในการพัฒนาการรักษาใหม่ที่มีประสิทธิภาพจำเป็นต้องมีความเข้าใจเชิงลึกถึงพยาธิสภาพของโรคนั้นๆ เมื่อเร็ว ๆ นี้ มีงานวิจัยรองรับว่าไมโครอาร์เอ็นเอ (miRNAs) มีบทบาทสำคัญในการกำเนิดมะเร็ง ซึ่งรวมถึงมะเร็งเซลล์ตับด้วย การวิเคราะห์ทางชีวสารสนเทศของเราได้แสดงให้เห็นว่าไมโครอาร์เอ็นเอแปดแปดห้าห้าพี (hsa-miR-885-5p) เป็นไมโครอาร์เอ็นเอ ที่มีศักยภาพในการเป็นไมโครอาร์เอ็นเอที่ยับยั้งการเกิดมะเร็ง เนื่องจากมีปริมาณการแสดงออกที่ลดลงในเนื้อเยื่อมะเร็งเซลล์ตับเมื่อเทียบกับเนื้อเยื่อปกติ โดยเฉพาะอย่างยิ่งในมะเร็งที่อยู่ในระยะรุนแรงกว่าจะยิ่งพบการแสดงออกที่ลดลงเมื่อเทียบกับมะเร็งที่อยู่ในระยะเริ่มต้น การค้นพบที่น่าสนใจนี้กระตุ้นให้เราตรวจสอบผลของไมโครอาร์เอ็นเอแปดแปดห้าห้าพีในมะเร็งเซลล์ตับ ในการวิจัยของเราทำให้ทราบว่าไมโครอาร์เอ็นเอแปดแปดห้าห้าพีสามารถยับยั้งการเพิ่มจำนวนเซลล์ได้อย่างมีประสิทธิภาพและขัดขวางการเข้าสู่ระยะ S จากระยะ G1 ซึ่งถือว่าเป็นขั้นตอนสำคัญในการเริ่มต้นการเพิ่มจำนวนของเซลล์ จากการวิเคราะห์โดยการทำนายเป้าหมายของไมโครอาร์เอ็นเอ เราสามารถระบุ CDK6 ซึ่งเป็นยีนที่เกี่ยวข้องกับการเข้าสู่ระยะ S ว่าเป็นเป้าหมายที่เป็นไปได้ของไมโครอาร์เอ็นเอแปดแปดห้าห้าพี การทดลองเพิ่มเติมช่วยยืนยันว่าไมโครอาร์เอ็นเอแปดแปดห้าห้าพีสามารถจับกับ CDK6 ได้โดยตรง ซึ่งนำไปสู่การลดระดับการแสดงออกในระดับยีนและโปรตีน นอกจากนี้เรายังได้ดำเนินการวิเคราะห์ลำดับเบสของอาร์เอเอ ซึ่งไม่เพียงแต่สนับสนุนว่าไมโครอาร์เอ็นเอแปดแปดห้าห้าพี มีส่วนร่วมในกระบวนการวัฏจักรของเซลล์เท่านั้น แต่ยังบ่งชี้ถึงศักยภาพของไมโครอาร์เอ็นเอแปดแปดห้าห้าพี ในฐานะตัวควบคุมเชิงลบของการเปลี่ยนเข้าสู่ระยะ S ของเซลล์ ซึ่งการค้นพบทั้งหมดนี้แสดงให้เห็นถึงบทบาทหน้าที่ที่น่าสนใจของไมโครอาร์เอ็นเอแปดแปดห้าห้าพีในมะเร็งเซลล์ตับ โดยอาจทำงานผ่านการควบคุม CDK6 ดังนั้นการตรวจสอบเพิ่มเติมเกี่ยวกับหน้าที่เพิ่มเติมและศักยภาพในการรักษาของไมโครอาร์เอ็นเอแปดแปดห้าห้าพีจึงมีความสำคัญอย่างยิ่ง เพื่อที่เราจะได้เข้าถึงศักยภาพของไมโครอาร์เอ็นเอแปดแปดห้าห้าพีในการรักษามะเร็งเซลล์ตับ

สาขาวิชา ชีวเคมีทางการแพทย์
ปีการศึกษา 2565

ลายมือชื่อนิสิต
ลายมือชื่อ อ.ที่ปรึกษาหลัก

6470105730 : MAJOR MEDICAL BIOCHEMISTRY

KEYWORD: Hepatocellular carcinoma, miRNA, miR-885-5p, CDK6

Archittapon Nokkeaw : Exploring roles of miR-885-5p in hepatocellular carcinoma. Advisor:
CHAIYABOOT ARIYACHET, Ph.D.

Hepatocellular carcinoma (HCC), the most prevalent form of liver cancer, exerts a significant burden on Southeast Asian countries and stands as the third leading cause of cancer-related mortality worldwide. Despite this alarming impact, effective treatments for HCC are lacking, resulting in low survival rates and high recurrence rates. Therefore, a comprehensive understanding of the disease's underlying mechanisms is crucial for the development of novel and potent therapies. Recently, it has been recognized that microRNAs (miRNAs) play a vital role in tumorigenesis, including HCC. Our bioinformatic analysis has highlighted hsa-miR-885-5p as a potential candidate miRNA due to its downregulation in HCC tissue compared to normal tissue, particularly in higher-grade tumors. This intriguing finding prompted our study to investigate the function of hsa-miR-885-5p in HCC. In our research, we employed functional assays to demonstrate that hsa-miR-885-5p effectively suppresses cell proliferation and hinders the critical G1/S transition, a crucial step initiating cell proliferation. Through meticulous miRNA target prediction analysis, we identified CDK6, a gene associated with the G1/S transition, as a potential target of hsa-miR-885-5p. Further experimental validation confirmed that hsa-miR-885-5p directly targets CDK6, leading to reduced expression levels and perturbations in protein levels. Moreover, we conducted RNA-seq analysis, which not only supported the involvement of hsa-miR-885-5p in cell cycle processes but also indicated its potential as a negative regulator of the G1/S transition. These findings collectively highlight the interesting role of hsa-miR-885-5p in HCC, potentially through its interaction with CDK6. Consequently, further investigations into the precise functions and therapeutic potential of hsa-miR-885-5p are warranted to unlock its full therapeutic value in HCC.

CHULALONGKORN UNIVERSITY

Field of Study: Medical Biochemistry

Student's Signature

Academic Year: 2022

Advisor's Signature

ACKNOWLEDGEMENTS

I would like to express my deepest gratitude to Dr. Chaiyaboot Ariyachet for his invaluable guidance and support as my advisor throughout the completion of my master's degree thesis. Dr. Ariyachet's expertise and dedication to scientific research have been instrumental in shaping my skills and refining my approach to academic inquiry. His insightful feedback, encouragement, and patience have been crucial in guiding me towards achieving a higher level of excellence in my work.

I would also like to extend my heartfelt appreciation to the members of the Center of Excellence in Hepatitis and Liver Cancer at the Faculty of Medicine, Chulalongkorn University. Their unwavering support and assistance have played a vital role in the successful completion of my research. Their extensive knowledge, resources, and willingness to share their expertise have greatly enhanced the quality and depth of my study. I am grateful for their collaborative spirit and the opportunity to learn from their collective wisdom.

Lastly, I would like to thank the Faculty of Medicine, Chulalongkorn University for providing me with an exceptional academic environment and the necessary resources to pursue my research endeavors. The vibrant and stimulating atmosphere fostered by the institution has undoubtedly contributed to my personal and intellectual growth.

I am humbled and deeply appreciative of the contributions made by Dr. Chaiyaboot Ariyachet and the members of the Center of Excellence in Hepatitis and Liver Cancer. Their unwavering support, guidance, and expertise have been invaluable in the successful completion of my master's degree thesis. I will forever be grateful for their mentorship and the knowledge I have gained through their collaboration.

Archittapon Nokkeaw

TABLE OF CONTENTS

	Page
ABSTRACT (THAI).....	iii
ABSTRACT (ENGLISH).....	iv
ACKNOWLEDGEMENTS.....	v
TABLE OF CONTENTS.....	vi
LIST OF TABLES.....	ix
LIST OF FIGURES.....	x
Chapter 1 Background.....	1
Introduction.....	1
Research question.....	4
Hypothesis.....	4
Objectives.....	4
Chapter 2 Literature review.....	5
Primary liver cancer.....	5
Hepatocellular carcinoma (HCC).....	6
Major risk factors for HCC.....	8
<u>Hepatitis B virus</u>	8
<u>Hepatitis C virus</u>	9
<u>Alcohol</u>	11
<u>Aflatoxin B1</u>	13
<u>Obesity</u>	14
<u>Diabetes mellitus</u>	16

Current treatment for HCC.....	17
miRNAs and HCC	20
<u>The role of miRNAs in HCC</u>	22
Tumor suppressor genes.....	22
Oncogenes	23
miRNAs as a potential therapeutic in HCC.....	23
Cell cycle and cancer initiation and progression	23
G1-S phase transition	25
Chapter 3 Conceptual framework.....	28
Chapter 4 Research workflow.....	29
Research workflow for the selecting candidate miRNA.....	29
Research workflow for investigate miRNA-mRNA axis	30
Chapter 5 Research methodology.....	31
MicroRNA expression profile analysis.....	31
Cells.....	31
qRT-PCR analysis for miRNA expression.....	33
Overexpression of miRNA.....	34
MTT assay for cell proliferation	36
BrdU assay	37
Cell cycle analysis.....	38
qRT-PCR analysis for candidate target proteins expression	39
Dual luciferase assay	40
Protein extraction	41
Bradford assay for determining protein concentration	41

Western blot	42
Sample preparation for RNA-Seq.....	43
GO term and pathway analysis	44
Statistical analysis	44
Chapter 6 Results	45
MicroRNA expression profile analysis identified hsa-miR-885-5p as a candidate miRNA.....	45
Hsa-miR-885-5p is highly downregulated in cancer cell.....	47
Hsa-miR-885-5p suppresses the growth of HCC cells <i>in vitro</i>	48
Hsa-miR-885-5p inhibits the G1/S transition of HCC cells	50
<i>CDK6</i> is predicted as a hsa-miR-885-5p target	54
Hsa-miR-885-5p directly interacts with the 3'UTR of <i>CDK6</i> transcripts	56
Overexpression of hsa-miR-885-5p inhibits expression of <i>CDK6</i>	57
RNA-Seq analysis identified the G1/S transition as a potential pathway for hsa-miR- 885-5p in HCC.....	59
Chapter 7 Discussion and Conclusion	64
Appendix	73
REFERENCES	79
VITA.....	92

LIST OF TABLES

	Page
Table 1 The top 10 countries with the highest estimated age-standardized incidence rates (ASR) in the world.....	7
Table 2 Benefits and drawbacks of each treatment option for HCC.....	18
Table 3 Characteristics of HCC cell lines.....	32
Table 4 Primer's sequence used for miRNA expression analysis.....	34
Table 5 Primer's sequence used for miRNA target expression analysis.....	40
Table 6 The lists of G1/S predicted targets of hsa-miR-885-5p.....	55
Table 7 Lists of mRNAs targeted by E2F that are downregulated in RNA-seq and their functions.....	62

LIST OF FIGURES

	Page
Fig. 1 Estimated age-standardized incidence rates (World) in 2020.....	7
Fig. 2 Mechanisms of some risk factors in hepatocellular carcinoma tumorigenesis.....	9
Fig. 3 Global incidence rates of liver cancer, prevalence of chronic HCV infection and chronic HBV infection	11
Fig. 4 Burden of HCC due to obesity.....	15
Fig. 5 Biogenesis pathway of miRNA.....	21
Fig. 6 Phases of the cell cycle	24
Fig. 7 The role of cyclin/CDK complexes in cell cycle progression	27
Fig. 8 Preliminary analysis of downregulated miRNAs in HCC.....	46
Fig. 9 Expression level of hsa-miR-885-5p in HCC cell lines (HepG2, JHH-4, and SNU-449).....	47
Fig. 10 Hsa-miR-885-3p attenuates cells growth in vitro.....	49
Fig. 11 BrdU incorporation assay of HepG2.....	51
Fig. 12 BrdU incorporation assay of JHH-4.....	52
Fig. 13 BrdU incorporation assay of SNU-449.....	53
Fig. 14 Cell cycle analysis of JHH-4 cells.....	53
Fig. 15 CDK6 is a direct target of hsa-miR-885-5p.....	57
Fig. 16 Hsa-miR-885-5p inhibits expression of CDK6.....	58
Fig. 17 Proposed mechanism of hsa-miR-885-5p in promoting proliferation of HCC cells via targeting <i>CDK6</i>	59
Fig. 18 GO term and pathway analysis of genes obtained from RNA-seq comparison between JHH-4 expressing hsa-miR-885 and control.....	60

Fig. 19 Volcano plot displaying RNA-seq data. 61



Chapter 1 Background

Introduction

Hepatocellular carcinoma (HCC) is the most frequently diagnosed type of liver cancer, accounting for approximately 90 percent of all cases [1]. Virtually all cirrhosis-inducing conditions can give rise to HCC, including prolonged infection with hepatitis B and C viruses (HBV and HCV), chronic alcohol consumption, an aflatoxin-B1-contaminated diet, and non-alcoholic fatty liver disease [2]. Globally, liver cancer is a significant concern for the healthcare system, as the World Health Organization (WHO) estimated that more than 905,000 individuals had been diagnosed with the disease and more than 830,000 had died in 2020. Liver cancer was placed sixth in terms of incidence and third in terms of death when compared to other types of cancer [3]. Additionally, the incidence and mortality of liver cancer will continue to rise year after year, to the point where about 1.4 million individuals will have liver cancer and 1.3 million will die annually from liver cancer by 2040 [4]. Although therapy for HCC has made significant progress over the past four decades, many patients still have a low 10-year survival rate and a high likelihood of HCC recurrence within 5 years [5]. Therefore, gaining a comprehensive understanding of the processes and pathogenesis of HCC is pivotal for the development of innovative treatment strategies.

MicroRNAs (miRNAs) represent a class of small, noncoding RNAs that play a crucial role in the regulation of gene expression [6]. The biogenesis of canonical miRNAs encompasses various intricate processes [6, 7]. Initially, miRNAs are transcribed as primary miRNAs (pri-miRNAs) from genes encoding miRNAs by RNA polymerase II. Subsequently, Drosha mediates the conversion of pri-miRNAs into precursor miRNAs (pre-miRNAs), which are subsequently transported to the cytoplasm and processed by Dicer. This processing eliminates the terminal loop, resulting in the generation of a mature miRNA duplex. The mature miRNA duplex is then incorporated into proteins of the Argonaute (AGO) family. AGO2 cleaves the miRNA passenger strands, which are subsequently eliminated by cellular machinery to form mature single-strand miRNA. Consequently, miRNA-induced silencing complexes (miRISC) are formed, facilitating the recognition of target mRNA and subsequent suppression of target gene expression via mRNA degradation or translational repression. Incomplete complementary binding leads to translational repression or deadenylation of the target mRNA, while perfect complementary binding triggers degradation of the target mRNA [7]. Several studies have reported alterations in miRNA expression during HBV and HCV infection [7, 8]. Furthermore, evidence suggests that ethanol consumption may impact miRNA levels [9, 10]. Multiple studies have established a connection between the detrimental effects of aflatoxin B1 and changes in miRNA expression [11]. Consequently, dysregulation of

miRNAs may exert a substantial influence on the pathophysiological processes underlying human malignancies.

The bioinformatic analysis revealed a significant downregulation of hsa-miR-885-5p in the tumor tissue compared to the normal tissue of hepatocellular carcinoma (HCC) patients. Furthermore, a notable decrease in hsa-miR-885-5p expression was observed in high-grade tumor tissue when compared to low-grade tumor tissue. These preliminary findings strongly suggest the crucial involvement of hsa-miR-885-5p in the progression and development of HCC. Consequently, this study aims to delve deeper into the investigation of the role played by hsa-miR-885-5p in HCC.

The current understanding of HCC, particularly in relation to miR-885-5p and its implications in HCC pathogenesis, is limited. Therefore, this research endeavor seeks to enhance our comprehension of miRNAs and their functionality within the context of HCC.

Research question

- 2.1 Can miR-885-5p suppress cell proliferation?
- 2.2 What is the target of miR-885-5p to suppress cell growth?

Hypothesis

- 3.1 MiR-885-5p could inhibit cell growth.
- 3.2 MiR-885-5p can downregulate genes associated with the proliferation of HCC.

Objectives

- 1.1 To evaluate the roles of miR-885-5p in HCC.
- 1.2 To identify the mRNA target of miR-885-5p in HCC.

Chapter 2 Literature review

Primary liver cancer

Primary liver cancer is recognized as the sixth most prevalent form of cancer globally, encompassing approximately 4.7% of all cancer-related incidents and 8.3% of all cancer-related mortalities [3]. Within developed nations, its incidence remains relatively low, with an estimated 199,931 new cases reported, constituting 22.1% of all newly diagnosed cases. Conversely, liver cancer exhibits a considerably higher prevalence within the developing world, accounting for 77.9% (705,416 new cases estimated) of reported cases, particularly prevalent in Sub-Saharan Africa, East and Southeast Asia, Melanesia, and Micronesia/Polynesia [12-14]. This discrepancy can primarily be attributed to the prominent environmental risk factors for liver cancer, namely chronic hepatitis B virus (HBV) infection and dietary consumption of aflatoxin B1-contaminated foods [15-19]. These risk factors are more prevalent in low-income countries [20]. In Thailand, liver cancer represents the most commonly diagnosed cancer type, with an estimated 27,394 new cases projected for the year 2020. Among the Thai population, it is the most frequently occurring cancer among males and the fourth most prevalent among females. Moreover, liver cancer stands as the leading cause of cancer-related mortality for both genders in Thailand, resulting in the loss of 26,704 lives in 2020 [12].

Hepatocellular carcinoma (HCC)

The majority of primary liver cancers are dominated by HCC, which accounts for approximately 90% of all cases [1]. Geographical differences affect the distribution of HCC due to the variability of underlying risk factors [21]. HCC was expected to occur 72% in Asia, where most of the cases happen in China (more than 60% of all cases in Asia), while Mongolia has the highest incidence rate in the world (85.6 per 100,000) (Fig. 1) [12]. Globally, Thailand is one of the four Southeast Asian countries that rank among the top ten countries with the highest incidence rates (Table 1) [12]. Incidence and mortality rates are approximately identical as a consequence of the poor prognosis, the associated underlying liver disease, the aggressiveness of the cancer, and the limited therapeutic options [22]. In high-prevalence regions, HCC has been diagnosed in children as young as 5 months [23]. Generally, up until the age of 75, the incidence rates of HCC are often directly associated with age [24]. HCC exhibits a clear predilection toward men. In low-incidence areas, men are four times more likely than women to develop HCC. In high-incidence areas, HCC is eight times more likely to occur in men than in women [25]. Chronic liver disease is observed in more than 90% of HCC cases [1]. The greatest risk factor for HCC is cirrhosis of any etiology. HCC is the predominant source of mortality in cirrhotic patients.

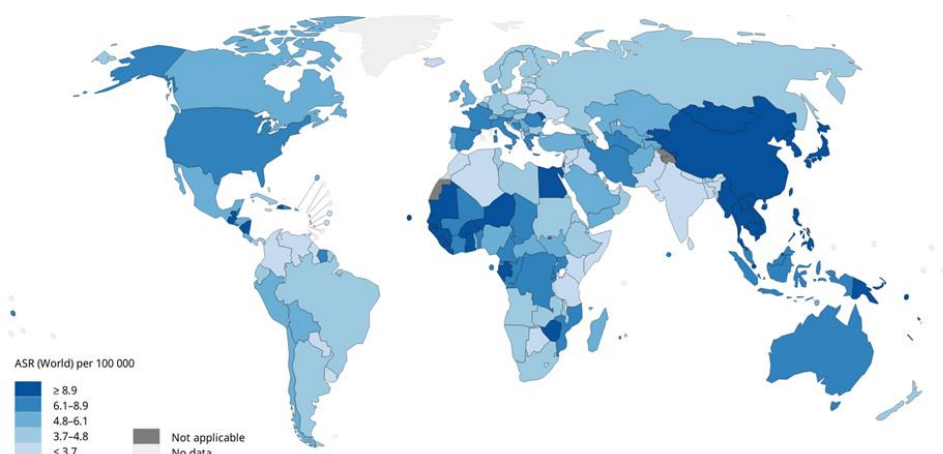


Fig. 1 Estimated age-standardized incidence rates (World) in 2020 [12].

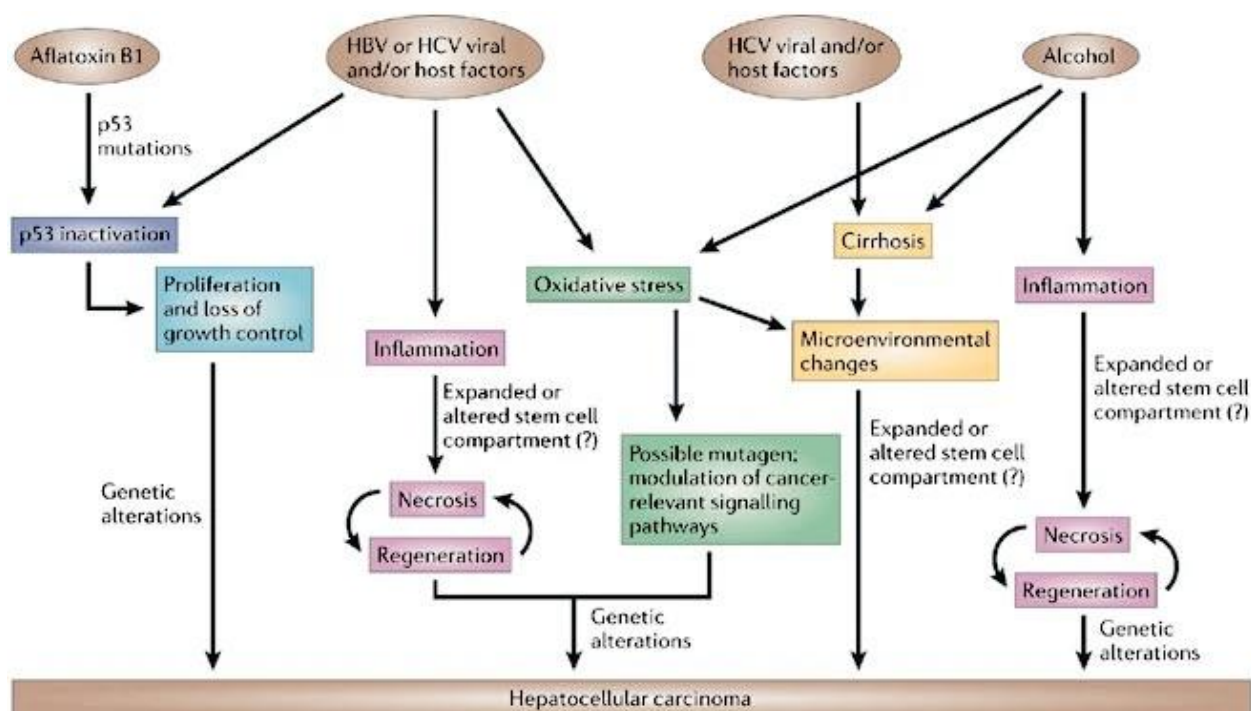
Table 1 The top 10 countries with the highest estimated age-standardized incidence rates (ASR) in the world[12].

Country	ASR per 100,000
Mongolia	85.6
Egypt	34.1
Lao People's Democratic Republic	24.4
Cambodia	24.3
Viet Nam	23
Thailand	22.6
Guinea	21.8
China	18.2
The Republic of the Gambia	17.2
Ghana	16.9

Major risk factors for HCC

Hepatitis B virus

Infection with the Hepatitis B virus (HBV) constitutes the primary risk factor for the development of Hepatocellular Carcinoma (HCC) [26]. T-cell immune responses against viral infections contribute to the induction of inflammation, hepatocyte necrosis, and subsequent hepatocyte regeneration. This ongoing process can induce genetic alterations (Fig. 2) [2]. Approximately 2 billion individuals worldwide are afflicted with HBV, and it is responsible for 50% of HCC cases, making it one of the most prevalent carcinogens [27, 28]. HBV is a hepatotropic DNA virus with a partial double-stranded genome capable of integrating its genetic material into the host genome, thereby leading to insertional mutagenesis and activation of oncogenes within the host cell [29]. HBV is also known to activate tumor-promoting signaling pathways, such as Wnt/ β -Catenin [30], PI3K/AKT [31], MAPK [32], and the oxidative stress pathway [33], thereby facilitating cancer initiation and progression. Moreover, components of HBV proteins have been observed to deactivate the p53 tumor suppressor gene, resulting in increased proliferation and impairment of DNA-damage checkpoints in host cells, thereby promoting the survival of cancer cells [34].



Copyright © 2006 Nature Publishing Group
Nature Reviews | Cancer

Fig. 2 Mechanisms of some risk factors in hepatocellular carcinoma tumorigenesis[2].

Hepatitis C virus



Chronic infections of Hepatitis B virus (HBV) and Hepatitis C virus (HCV) are accountable for three-quarters of Hepatocellular Carcinomas (HCCs). Consequently, regions exhibiting high rates of these infections often display elevated incidence rates of HCC, as depicted in Figure 3 [35]. HCV infection affects approximately 2.5% of the global population [36] and stands as the primary cause of HCC in western countries such as the United States, Europe, South America, and Japan [37]. Roughly 80–85% of individuals acutely infected with HCV are unable to eliminate the virus, resulting in chronic infection [38]. Chronic HCV infection fosters the emergence of inflammation-induced lesions within the liver, thereby leading to hepatic fat accumulation, known

as hepatic steatosis, and progressive fibrosis [39]. Over a span of 20–30 years, 20% of patients may develop liver cirrhosis [40]. Once cirrhosis has formed, the annual incidence of HCC development ranges from 1% to 4% [41]. HCV infection is associated with approximately 27% of cirrhosis cases and 25% of HCC cases [42]. Carcinogenesis can be facilitated by HCV through the indirect impact of chronic inflammation, which elevates levels of reactive oxygen species (ROS) that inflict damage upon hepatocytes at both the metabolic and genetic levels [43, 44]. Furthermore, HCV can directly contribute to the development of HCC by altering host regulatory mechanisms pertaining to cell growth, cell death, lipid metabolism, and blood vessel growth [44].



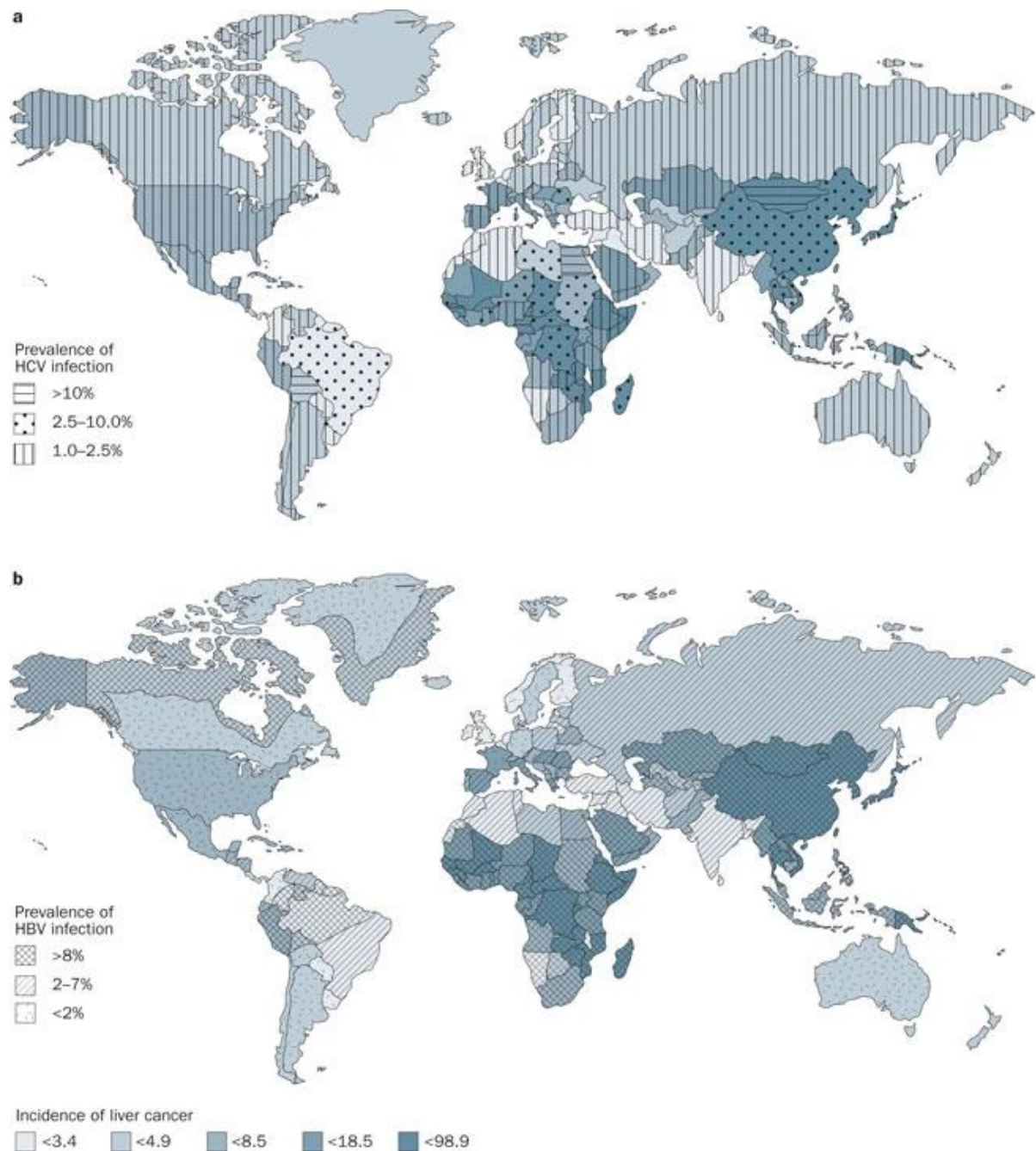


Fig. 3 Global incidence rates of liver cancer, prevalence of chronic HCV infection and chronic HBV infection[35].

Alcohol

It has been demonstrated that excessive alcohol consumption is a significant contributing factor to the occurrence of liver cirrhosis and hepatocellular carcinoma (HCC) [45]. The relationship between alcohol use and the development of cirrhosis

and HCC is estimated to exhibit a linear dose-dependent pattern [45]. Alcohol has the potential to directly contribute to the development of HCC through genotoxic effects on human cells as well as indirectly by causing cirrhosis [46]. The risk of developing cirrhosis increases when daily alcohol intake surpasses 20 grams over a period of more than ten years, whereas the risk of developing HCC increases with daily consumption exceeding 80 grams [47, 48]. It is noteworthy that alcohol is considered a more significant risk factor for HCC carcinogenesis in women compared to men [49]. Multiple studies have demonstrated that women exhibit greater susceptibility to the toxic effects of alcohol due to their lower activity of gastric alcohol dehydrogenase (ADH), leading to higher serum concentrations and a prolonged presence of alcohol in the bloodstream in comparison to men [50]. Ethanol undergoes metabolic conversion to acetaldehyde via both the canonical pathway involving ADH and the non-canonical pathway involving cytochrome P450 2E1 (CYP2E1) [51]. The CYP2E1-dependent pathway, which is active only under high ethanol levels, generates reactive oxygen species (ROS), including hydroxyethyl, hydroxyl radicals, and superoxide anions, capable of inducing cell death, DNA damage, and triggering tumorigenesis [52, 53]. Furthermore, CYP2E1 expression is approximately eight times higher in women than in men [52], resulting in increased ROS production and greater damage. Acetaldehyde, a metabolite of ethanol, exhibits high toxicity and is recognized as a carcinogen. Acetaldehyde induces point mutations, sister chromatid exchanges, and promotes the formation of adducts in

proteins and DNA [54]. The adduction of crucial proteins may lead to reduced catalytic activity and functional impairments, while DNA adducts can facilitate cancer development by inducing errors during DNA replication and mutations in oncogenes or tumor suppressor genes.

Aflatoxin B1

Aflatoxins, a difuranocoumarin derivative, are secondary fungal metabolites produced by the molds in the genus *Aspergillus*, particularly *A. flavus* and *A. parasiticus* [55]. They exhibit potent carcinogenic properties towards hepatocellular carcinoma (HCC) and are classified as group 1 carcinogens by the International Agency for Research on Cancer (IARC) [56]. Among the four known aflatoxins (B1, B2, G1, and G2), all have been demonstrated to be carcinogenic in both humans and animals, with aflatoxin B1 displaying the most profound hepatotoxicity and hepatocarcinogenicity [57].

A substantial portion of the global food supply, including rice, groundnuts, and corn, is contaminated with aflatoxin B1, primarily during the harvesting and storage stages, leading to adverse health effects [58]. Roughly 4.5 billion individuals are exposed to aflatoxin-contaminated foodstuffs on a regular basis [59]. Regions characterized by high temperatures and humidity, such as Southeast Asia and Sub-Saharan Africa, frequently exhibit elevated aflatoxin contamination levels due to the conducive conditions for fungal growth [60].

Aflatoxin can induce gene mutations by facilitating the formation of DNA adducts, which in turn activate proto-oncogenes and deactivate tumor suppressor genes, potentially culminating in the development of cancer [61, 62]. The metabolism of aflatoxin B1 by liver cytochrome P450 enzymes, particularly CYP3A4, can lead to the production of aflatoxin B1-8, 9-oxide (AFBO), an intermediate possessing genotoxic and carcinogenic properties [63]. This highly reactive substance can bind to hepatic DNA, resulting in the formation of DNA adducts [63]. In the absence of proper repair mechanisms prior to DNA replication, these adducts can induce genetic mutations. Aflatoxin exposure has been associated with mutations in the p53 tumor suppressor gene (Fig. 2) [2].

Obesity



Obesity is widely recognized as a significant risk factor for cancer, including primary liver cancer [64]. There is a growing incidence of hepatocellular carcinoma (HCC) in obese individuals. Men with a body mass index (BMI) ≥ 30 kg/m² have a significantly increased risk of mortality due to liver cancer compared to men with a normal body weight [65]. The likelihood of liver cancer-related death is 4.5 times higher in men with class 2 obesity (BMI ≥ 30 kg/m²) than in men with a healthy weight [66]. Obesity is strongly correlated with a higher prevalence of nonalcoholic fatty liver disease (NAFLD) [67]. NAFLD is characterized by the accumulation of lipids in hepatocytes [68] and is an umbrella term encompassing the liver manifestations of metabolic syndrome [69]. It encompasses various liver conditions such as benign

steatosis, steatohepatitis, cirrhosis, and, in some cases, hepatocellular carcinoma [69]. Non-alcoholic steatohepatitis (NASH) is a necroinflammatory subtype of NAFLD characterized by inflammation and liver damage [70]. NASH can progress to fibrosis and cirrhosis [71]. In the near future, NASH may surpass viral hepatitis as the leading cause of liver cirrhosis [72]. Figure 4 illustrates the association between obesity, NAFLD, NASH, cirrhosis, and HCC [73]. Recently, molecular mechanisms underlying obesity-related HCC have been elucidated. These mechanisms include chronic inflammation resulting from adipose tissue remodeling, ectopic lipid accumulation leading to cellular lipotoxicity, insulin resistance resulting in elevated insulin and insulin-like growth factor levels, and impaired senescence in stellate cells [73, 74]. The deposition of excessive fat leads to adipose tissue expansion [75, 76]. This process involves extensive tissue remodeling, resulting in a significantly altered pattern of adipokine release by adipocytes, which can impact tumorigenesis, metastasis, and chemoresistance through various signaling pathways [76, 77].

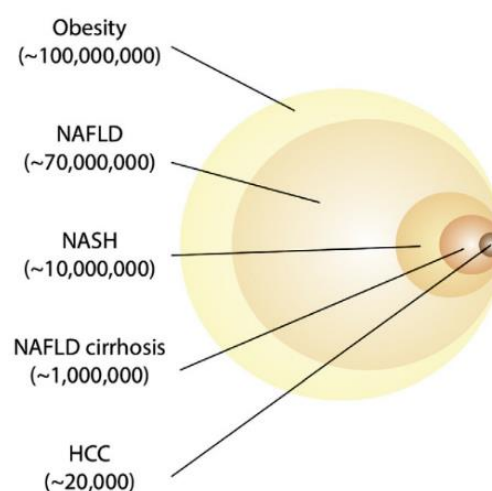


Fig. 4 Burden of HCC due to obesity[73].

Diabetes mellitus

Diabetes mellitus (DM) is a metabolic disorder characterized by persistent hyperglycemia, aberrations in carbohydrate, lipid, and protein metabolism, inadequate insulin secretion, and/or insulin resistance. Diabetes affects approximately 9% of the global population and is projected to impact 700 million individuals by the year 2045 [78]. A robust correlation exists between diabetes mellitus and hepatocellular carcinoma (HCC) [79]. Individuals with diabetes face an elevated risk, two- to threefold higher, of developing HCC, particularly those with type 2 diabetes [80, 81]. This association may be attributed to the impact of free fatty acids, which induce insulin resistance and hyperglycemia, thereby necessitating the production of hyperinsulinemia as a compensatory response to insulin resistance [82]. Hyperinsulinemia, in turn, stimulates the secretion of proinflammatory cytokines. Furthermore, hyperglycemia leads to the release of free fatty acids, resulting in the accumulation of reactive oxygen species (ROS) [80]. Both proinflammatory cytokines and ROS have the potential to instigate carcinogenesis via chronic inflammation, thereby activating a cellular cascade implicated in malignant transformation [80, 83]. Additionally, the binding of insulin to its receptor triggers the activation of the phosphatidylinositol 3-kinase (PI3K)-AKT and Ras/mitogen-activated protein kinase (MAPK) pathways, which are closely associated with cell survival and proliferation [80, 84].

Current treatment for HCC

There are numerous treatment options available for hepatocellular carcinoma (HCC). The selection of an appropriate treatment modality relies on various determining factors, such as the tumor's size and location, cancer staging, and the patient's overall health condition [85]. For early and intermediate stages of HCC, potential treatment options encompass surgical intervention, liver transplantation, ablation techniques, and embolization procedures. In cases of advanced HCC, patients are typically treated with chemotherapy, targeted therapy, or immunotherapy [86].



Table 2 Benefits and drawbacks of each treatment option for HCC.

Treatment option	Benefits	Drawbacks
Surgery	Often the most effective treatment for early-stage HCC.	It may not be suitable for patients with underlying liver dysfunction or locally advanced disease.
Liver transplantation	Considered one of the most effective treatments with a high survival rate.	The availability of transplantable livers is limited and the criteria for patients who can undergo the procedure are very restrictive. Only a small number of patients can receive this treatment.
Ablation	Minimally invasive procedure that can be performed on an outpatient basis. It can provide a cure for small, very early-stage patients who are not candidates for liver transplant.	Not suitable for larger tumors or metastatic tumors.
Embolization	Minimally invasive procedure. It can help control the symptoms of advanced HCC by blocking the blood supply to the cancerous tissue	May cause post-embolization syndrome, such as abdominal pain, iatrogenic bile duct injury, hypoxic cholecystitis, and liver abscess.

Treatment option	Benefits	Drawbacks
Chemotherapy	Can help control the symptoms of advanced HCC.	Many side effects make these treatments poorly tolerated by patients with liver cirrhosis. Furthermore, these treatments can also cause damage to healthy cells and organs.
Targeted therapy	Generally, these treatments are better tolerated than chemotherapy and may have fewer side effects.	Targeted therapy may not be effective for all people with HCC due to therapeutic resistance.
Immunotherapy		Unpredictable efficacy necessitates the identification of additional biomarkers and cancer pathways. The cost of the treatment is high, making it inaccessible to those who need it.

Despite the recent advancements in the treatment of HCC, achieving a complete cure for this malignancy remains a considerable challenge. While these therapeutic interventions demonstrate efficacy in managing HCC symptoms and prolonging overall survival, they typically do not possess curative potential. Consequently, it is crucial for individuals afflicted with HCC to receive continuous

medical care and diligent monitoring to effectively manage the disease and its associated complications.

miRNAs and HCC

MiRNAs are small, non-coding RNA molecules approximately 23 nucleotides in length that fulfill crucial roles in the regulation of gene expression by specifically binding to target messenger RNAs (mRNAs) and inhibiting their translation into proteins [87]. Figure 5 presents an illustrative depiction of the biogenesis pathway of miRNAs. In brief, pri-miRNAs are transcribed from their respective genes and subsequently processed into pre-miRNAs by the microprocessor complex, comprising the RNA-binding protein DiGeorge Syndrome Critical Region 8 (DGCR8) and a ribonuclease III enzyme called Drosha. The pre-miRNAs are subsequently exported to the cytoplasm via exportin 5 (XPO5) in a RanGTP-dependent manner, where they undergo further processing to generate the mature miRNA duplex with the aid of DICER1. The selection of the strand is based on its stability, with the more stable or functionally active strand being incorporated into the RNA-induced silencing complex (RISC) to form miRISC [6, 88]. Conversely, the less stable miRNA strand, also known as the passenger strand and denoted by an asterisk (*), undergoes degradation [89]. By associating with the AGO protein family, miRNAs within the miRISC complex can bind to the 3' untranslated region (UTR) of target mRNA molecules, resulting in mRNA degradation and/or translational repression [6, 90, 91]. The dysregulation of miRNA expression has been implicated in the development and progression of various

diseases, including hepatocellular carcinoma (HCC), through the alteration of gene expression involved in carcinogenesis.

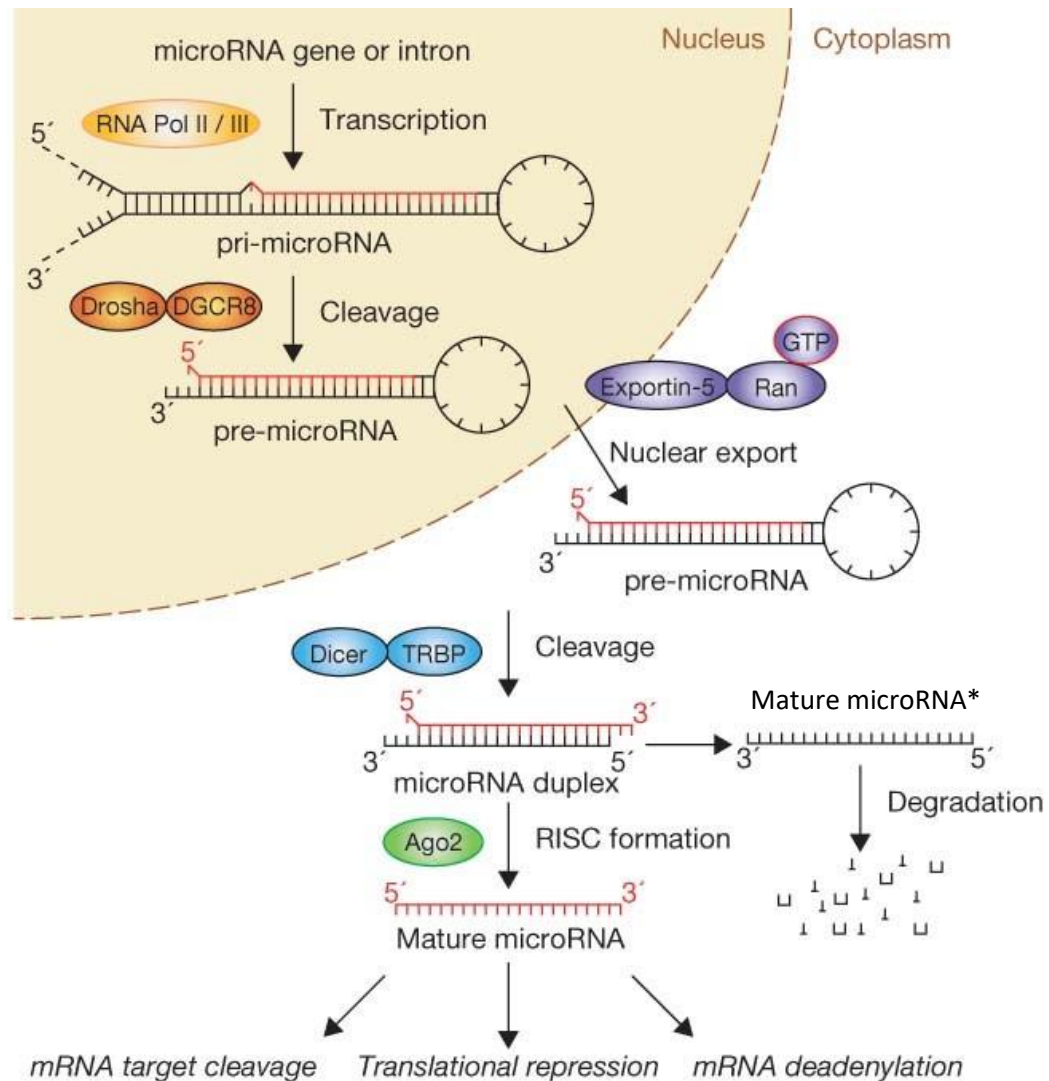


Fig. 5 Biogenesis pathway of miRNA. Adapted from [92].

Certain miRNAs have consistently exhibited upregulation or downregulation in hepatocellular carcinoma (HCC), indicating their potential involvement in the pathogenesis and progression of this disease. Extensive evidence supports the impact of miRNAs on various HCC processes, encompassing cell proliferation, apoptosis, angiogenesis, epithelial-mesenchymal transition, drug resistance, autophagy, and

metastasis [93]. Consequently, miRNAs have emerged as promising therapeutic targets in HCC treatment. Advancing our comprehension of the precise roles of miRNAs in this disease will facilitate the development of novel therapeutic approaches. However, further investigations are warranted to comprehensively elucidate the multifaceted roles of miRNAs in HCC and ascertain their full therapeutic potential.

The role of miRNAs in HCC

The roles of miRNAs in HCC are complex and multifaceted, and miRNAs have been found to have both tumor suppressor and oncogenic roles in the development of HCC.

Tumor suppressor genes

Certain miRNAs exhibit tumor-suppressive properties by inhibiting the expression of oncogenes and preventing the onset of HCC. The downregulation of these miRNAs can facilitate tumor progression by upregulating oncogene expression. For instance, miR-15 and miR-16-1 induce apoptosis by suppressing Bcl-2, an anti-apoptotic protein [94]. Furthermore, miR-139 inhibits HCC carcinogenesis by suppressing the expression of topoisomerase I (TOP1), a crucial factor in DNA replication [95]. Notably, diminished expression of miR-708 has been observed in HCC, and its overexpression significantly impedes HCC cell proliferation, migration, and invasion, plausibly by targeting SMAD3 [96].

Oncogenes

Conversely, certain miRNAs exhibit oncogenic properties by promoting the expression of oncogenes, thus contributing to HCC carcinogenesis. Overexpressing miR-129-5p in HCC cells downregulates bone morphogenetic protein 2 (BMP2) and augments HCC proliferation and metastasis [97]. Additionally, miR-92b directly targets SMAD7, a tumor suppressor gene, thereby stimulating HCC cell proliferation and metastasis [98]. Another miRNA, miR-130b-3p, upregulates endothelial markers CD31 and CD34 by targeting HOXA5, thereby fostering HCC angiogenesis, tumor progression, and reducing overall survival [99].

miRNAs as a potential therapeutic in HCC

The dysregulation of specific miRNAs in various cancers, including HCC, underscores their significant roles in tumorigenesis and progression. Consequently, manipulating the expression of cancer-associated miRNAs through antagonist miRNAs (antimiRs) and miRNA mimics holds promise as a next-generation therapeutic approach for addressing the pressing medical needs associated with advanced tumors [100].

Cell cycle and cancer initiation and progression

The cell cycle is a meticulously regulated system incorporating numerous evolutionarily conserved mechanisms for controlling cellular growth and division. It encompasses four distinct phases, namely G1, S, G2, and M. Collectively, G1, S, and G2 are referred to as interphase. In the initial G1 phase, the cell orchestrates

essential processes to facilitate DNA replication, including protein and RNA synthesis as well as organelle production, while simultaneously assessing its readiness for DNA synthesis. The subsequent S phase entails the replication of DNA. During the G2 phase, the cell undergoes genetic material reorganization and condensation in preparation for mitosis. The M phase, constituting the final stage of the cell cycle, encompasses the occurrence of mitosis [101].

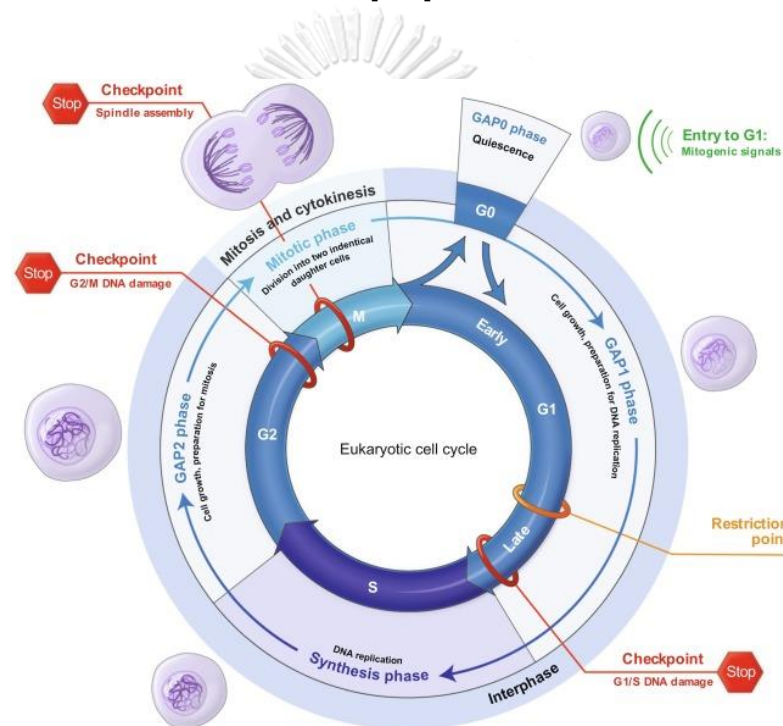


Fig. 6 Phases of the cell cycle[102].

The cell cycle is commonly dysregulated in cancer cells, leading to unrestricted cell proliferation. Cancer-associated mutations that disrupt cell cycle control enable persistent cell division, primarily by compromising the cells' ability to exit the cell cycle [103].

G1-S phase transition

The G1-S phase transition is a pivotal regulatory point in the cell cycle, possessing significant importance in academic research. During this transition, cells undergo a crucial determination of whether to enter the S phase and initiate DNA replication [104]. Several factors have the potential to influence the G1-S phase transition, including growth factors [105], cell-cycle regulators [106], and DNA damage [107]. Growth factors, as proteins, play a stimulating role in cellular expansion. The activation of the G1-S phase transition occurs upon the binding of growth factors to their corresponding receptors on the cell surface [105]. Cell-cycle regulators, which act as proteins, exert control over the progression of the cell cycle. They can either facilitate or impede the G1-S phase transition [106]. Moreover, damage to DNA can also lead to the occurrence of the G1-S phase transition. When DNA damage occurs, it initiates a signaling pathway that subsequently halts the G1 phase of the cell cycle [107].



The precise transition from the G1 to S phases of the cell cycle assumes paramount importance in regulating cell proliferation. Dysregulation of this transition can significantly contribute to the development of cancer. Within the G1 phase, cyclin-dependent kinase (CDK) activity, contingent upon growth-dependent conditions, promotes DNA replication and instigates the G1-to-S phase transition [104]. CDKs, as protein kinases, possess a distinct feature of relying on cyclin, a separate subunit that provides essential domains for enzymatic activity. CDKs fulfill

vital roles in governing cell division and transcription in response to various extracellular and intracellular signals [108].

The control of G1/S cell cycle checkpoints primarily rests upon the retinoblastoma protein (Rb) and E2F transcription factors. Rb, a critical cell cycle regulator, governs the G1/S transition by binding to and inhibiting the E2F transcription factor. Upon phosphorylation of Rb by CDKs, E2F is released, thus allowing E2F to activate the transcription of genes crucial for DNA replication and entry into the S phase. Two cell cycle kinase complexes, CDK4/6-Cyclin D and CDK2-Cyclin E, collaboratively phosphorylate Rb, relieving its inhibitory effect on E2F (Fig. 7) [109]. The activation of CDK4/6 leads to the partial phosphorylation of Rb, interfering with the Rb/E2F interaction and initiating E2F activity, along with the expression of CDK2 activators, cyclin E/A. Subsequent CDK2 activation induces complete phosphorylation (hyperphosphorylation) of Rb, establishing a CDK2-Rb positive feedback loop that propels the progression of the cell cycle [104, 109].

Given the significance of CDKs in the regulation of cell division, gene transcription, and other essential biological processes, researchers have proposed CDK inhibitors as potential treatments for cancer and other CDK-deficient diseases [110].

The deregulation of the G1-S phase transition constitutes a critical factor in the initiation and progression of cancer. By obtaining a comprehensive understanding

of the molecular mechanisms governing the G1-to-S phase transition, novel strategies for cancer prevention and treatment can be devised.

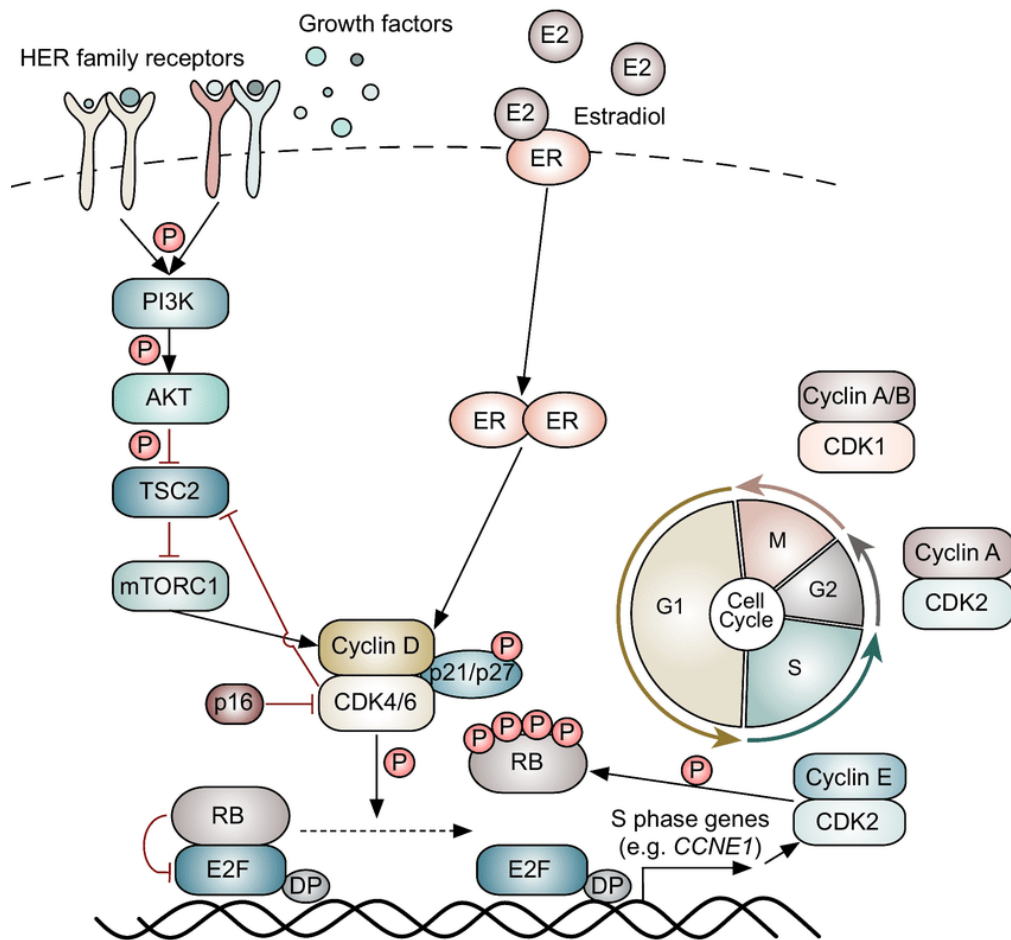


Fig. 7 The role of cyclin/CDK complexes in cell cycle progression[111].

Chapter 3 Conceptual framework

Knowledge of the role of miRNAs in HCC is needed for a better understanding of the nature of HCC



The development of an effective therapy depends critically on our understanding of the disease



The role of miRNAs in many cancers has been demonstrated in many studies



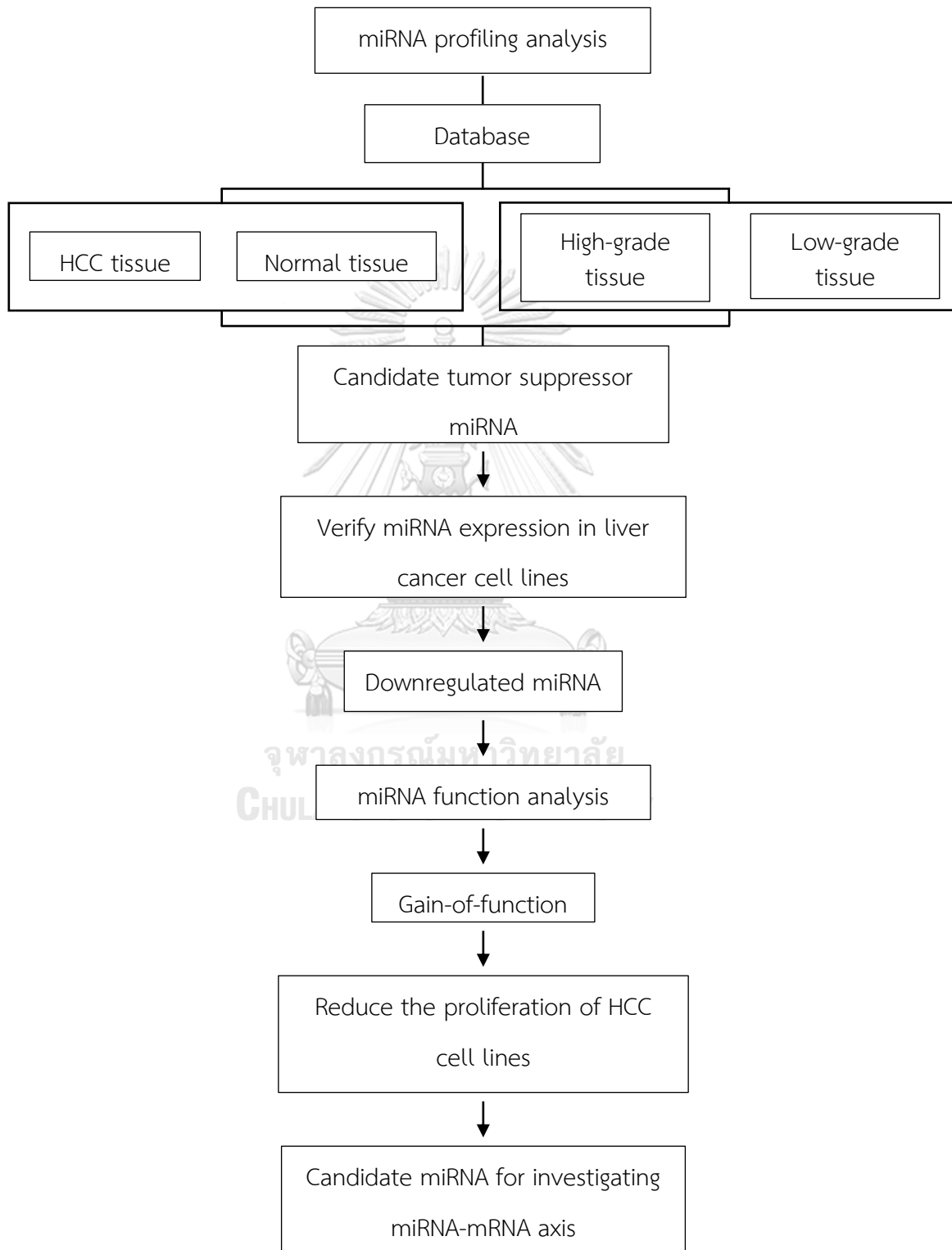
miRNAs that are downregulated in HCC when compared to normal cells can act as tumor suppressing miRNAs



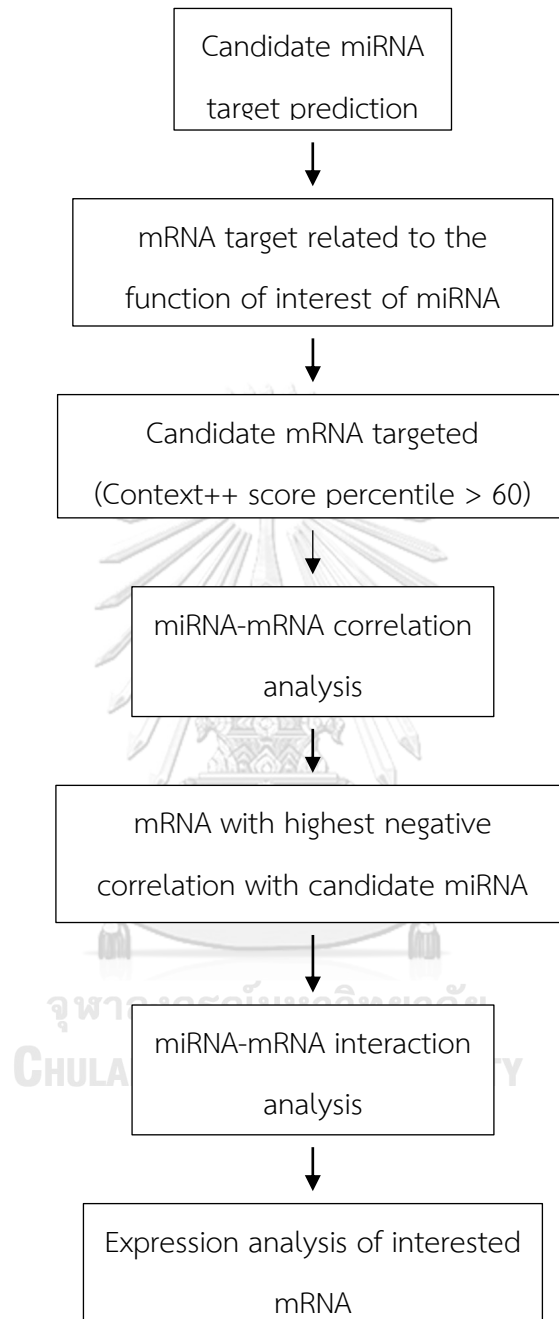
Investigating the relationship between miRNAs and HCC could help us understand the molecular mechanism of the cells in HCC

Chapter 4 Research workflow

Research workflow for the selecting candidate miRNA



Research workflow for investigate miRNA-mRNA axis



Chapter 5 Research methodology

MicroRNA expression profile analysis

The miRNA expression profiles in hepatocellular carcinoma (HCC) were obtained by retrieving data from the TCGA and GEO databases. In the GEO database, the search keyword 'hepatocellular carcinoma' was employed, followed by filtering the results based on organism (*Homo sapiens*) and study type (non-coding RNA profiling by array). Subsequently, any outcomes that did not involve a comparison between cancer tissue and normal tissue were excluded. The dataset with the largest number of samples, GSE147889, was selected for further analysis of differential expression. Additionally, the expression profiles from the TCGA database were analyzed, specifically comparing normal tissue with primary tumors and stage III tumors with stage I tumors, using the TCGAbiolinks package.

Cells

Cell lines HepG2, SNU-449, THLE-2, and HEK293T were procured from the American Type Culture Collection (ATCC). HepG2 originated from the liver hepatocellular carcinoma tissue of a 15-year-old male of Caucasian descent. SNU-449 was derived from hepatocellular carcinoma (HCC) tissue obtained from a 52-year-old Korean patient who tested positive for hepatitis B virus (HBV). JHH-4 was acquired from the Japanese Collection of Research Bioresources (JCRB) Cell Bank. This epithelial-like cell line was derived from the hepatocellular carcinoma tissue of a 51-year-old Japanese male patient, where neither HBV nor hepatitis C virus (HCV) were

observed. The Stbl3™ *E. coli* strain was provided by Thermo Fisher Scientific. HepG2 cell lines were cultured and maintained in Dulbecco's Modified Eagle's Medium (DMEM) with low glucose, supplemented with 10% fetal bovine serum (FBS), 1% L-glutamine, and 1% antibiotic-antimycotic (Gibco™, Thermo Fisher Scientific, Massachusetts, USA). Meanwhile, HEK293T cells were cultured and maintained in DMEM with high glucose, supplemented with 10% FBS, 1% L-glutamine, and 1% antibiotic-antimycotic. JHH-4 cells were cultured and maintained in Eagle's Minimum Essential Medium (EMEM) (Gibco™, Thermo Fisher Scientific, Massachusetts, USA) supplemented with 10% FBS, 1% L-glutamine, and 1% antibiotic-antimycotic. All cells were incubated at 37 °C with 5% CO₂ in a humidified atmosphere. The number of passages of cells used in all experiments did not exceed 20 passages. The characteristics of HCC cell lines are shown in Table 3.

Table 3 Characteristics of HCC cell lines.

Cell line	Origin	Viral status	Source
HepG2	Hepatocellular carcinoma of a 15-year-old, White, male youth with liver cancer	No evidence of Hepatitis B and C virus	ATCC
JHH-4	Hepatocellular carcinoma of a 51-year-old Japanese male	No evidence of Hepatitis B and C virus	JCRB
SNU-449	Primary hepatocellular carcinoma taken from a Korean patient	Hepatitis B virus was detected	ATCC

qRT-PCR analysis for miRNA expression

MiRNAs from four cell lines (THLE-2, SNU-449, HepG2, and JHH-4) were extracted using the GenUP™ Micro RNA Kit (Biotechrabbit, Berlin, Germany) according to the manufacturer's protocol. Subsequently, the miRNAs were reverse transcribed to cDNA by incorporating poly(U) at the 3' end of the miRNAs using 10x NEBuffer (New England Biolabs, Massachusetts, USA) (2.5 μ l), 50 mM UTP (Thermo Fisher Scientific, Massachusetts, USA) (0.25 μ l), 40 U/ μ l RiboLock (Thermo Fisher Scientific, Massachusetts, USA) (1 μ l), 500 ng miRNA, and nuclease-free water to achieve a final volume of 25 μ l. The mixture was incubated at 37 °C for 10 minutes, followed by the addition of 0.4 μ l of 10 μ M SL-PolyA, and incubated at 65 °C for 5 minutes. The reaction was then cooled on ice for 2 minutes. Next, 5xRT Buffer (Thermo Fisher Scientific, Massachusetts, USA) 8 μ l, 10 mM dNTPs 4 μ l, 200U RevertAid 2 μ l, and 40U/ μ l RiboLock 1 μ l was added to the mixture and incubated at 42 °C for 60 minutes followed by heat inactivation at 70 °C for 10 minutes. The final qPCR reaction mixture, of a 10 μ l final volume, contained 2.5 μ l of 4X CAPITAL™ qPCR Probe Master Mix (Biotechrabbit, Berlin, Germany), 0.25 μ l of each 10 μ M primer, and 6 μ l of nuclease-free water. The conditions of qPCR were 95 °C for 10 minutes, followed by 40 cycles of denaturation at 95 °C for 15 seconds, annealing at 55 °C for 15 seconds, and extension at 72 °C for 20 seconds. The qPCR was performed on a Life Technologies QuantStudio™ 3 real-time PCR system. The primer sequences employed in this study can be found in Table 4.

Table 4 Primer's sequence used for miRNA expression analysis.

miRNA name	Forward primer (5' → 3')	Reverse primer (5' → 3')
U6	CTCGCTTCGGCAGCACA	GCAGGGTCCGAGGTATTCG
hsa-miR-885-5p	TCCATTACACTACCCTGCCTCT	GCAGGGTCCGAGGTATTCG

Overexpression of miRNA

To investigate the gain-of-function of hsa-miR-885, the pri-miRNA sequence of hsa-miR-885 and its upstream and downstream sequences of approximately 200 base pairs were amplified from human genomic RNA through the process of PCR. The sequence of pri-miRNA was retrieved from The UCSC Genome Browser. The primers used in this step can be found in Table S1. The resultant PCR product was purified and subsequently ligated into the pLV-EF1 α -IRES-Puro plasmid (Addgene Plasmid #85132), which had been pre-digested with EcoRI and BamHI enzymes. The ligation reaction was conducted as follows: diluted oligo (0.5 μ l), gel-purified digested pLV-EF1 α -IRES-Puro (0.5 μ l), 10x ligase buffer (0.5 μ l), T4 DNA ligase (0.5 μ l), and water (3 μ l) were incubated at room temperature overnight. The resulting vectors were then introduced into Stbl3™ chemically competent *E. coli* cells, and the successful integration of the pri-miRNA was confirmed via colony PCR. Colony PCR reactions were carried out in a total volume of 12.55 μ l, comprising 1.25 μ l of 10x reaction buffer, 0.375 μ l of MgCl₂ (50 mM), 0.25 μ l of dNTPs (10 mM), 0.25 μ l of each primer (10 mM; Forward primer: 5'-TCAAGCCTCAGACAGTGGTTC-3', Reverse primer: 5'-

TCCATTACACTACCCTGCCTCT-3'), 0.05 μ l of Taq polymerase, and 10.125 μ l of nuclease-free water. The PCR reactions were carried out under the following conditions: initial denaturation at 95 °C for 2 minutes, followed by 35 cycles of denaturation at 95 °C for 30 seconds, annealing at 50 °C for 15 seconds, extension at 68 °C for 30 seconds, and a final extension step at 72 °C for 5 minutes. Positive clones were cultured in LB broth supplemented with ampicillin and incubated overnight at 30 °C. Plasmids from the positive *E. coli* clones were then purified using the ZymoPURE™ Plasmid Miniprep kit (Zymo Research, California, United States) according to the manufacturer's instructions. The identity of the pri-miRNA was confirmed via Sanger sequencing, utilizing the sequencing primer: 5'-TCAAGCCTCAGACAGTGGTTC-3'. Subsequently, the constructed vector was transfected into HCC cell lines. Lipid complexes were generated for transfection of the HCC cell lines using Lipofectamine 3000 transfection reagent (Invitrogen, Thermo Fisher Scientific, Massachusetts, USA). Initially, tube A was prepared by diluting 7 μ l of Lipofectamine 3000 in 250 μ l of Opti-MEM™ I medium. Tube B was then prepared by adding the pri-miRNA vector (2 μ g) and P3000 reagent (6 μ l) to 250 μ l of Opti-MEM™ I medium. The contents of tube A were added to tube B and incubated for 15 minutes at room temperature. Next, 1 ml of media was aspirated from the well, and 500 μ l of DNA-lipid complexes were added dropwise, followed by incubation for 6 hours at 37 °C and 5% CO₂. The media was subsequently replaced with fresh media and further incubated at 37 °C and 5% CO₂. After 48 hours, the media was replaced

with 2 ml of complete media supplemented with puromycin at concentrations of 1, 2, and 5 $\mu\text{g/ml}$ for the selection of HepG2, JHH-4, and SNU-449 cell lines, respectively, containing the pri-miRNA plasmid. The expression levels of hsa-miR-885-5p and the candidate target protein were assessed using quantitative PCR (qPCR), following the same methodology as previously described in the qRT-PCR analysis.

MTT assay for cell proliferation

HCC cell lines (5×10^4 cells/ml) were seeded onto 96-well plates, with each well containing a final volume of 100 μl . The plates were then incubated for the desired duration. MTT formazan (Sigma-Aldrich) was dissolved in DMEM (low glucose) to create a stock solution of 1 mg/100 μl . Subsequently, the stock solution was diluted with low-glucose DMEM to prepare an MTT solution with a concentration of 0.5 mg/ml. In each well, the culture medium was discarded and replaced with 100 μl of the 0.5 mg/ml MTT solution. The plate was incubated for 30 minutes at 37 °C with 5% CO_2 , after which the MTT solution was discarded. Next, the formazan crystals were solubilized by adding 100 μl of DMSO (Sigma-Aldrich) to each well. The plate was then incubated for an additional 5 minutes at 37 °C with 5% CO_2 , and thorough mixing was performed to ensure complete solubilization. Finally, the absorbance of all the samples was measured at 570 nm using a BioTek™ Synergy™ HTX Multi-Mode Microplate Reader (Biotek, Thermo Fisher Scientific, Vermont, USA).

BrdU assay

First, 100 mg of 5-bromo-2'-deoxyuridine (BrdU) was dissolved in 32.5 ml of dimethyl sulfoxide (DMSO) to prepare a 10 mM BrdU stock solution. Subsequently, the BrdU stock solution was diluted in the cell culture medium at a ratio of 1:1000, resulting in a BrdU labeling solution with a concentration of 10 μ M. For the preparation of the blocking buffer, 5% bovine serum albumin (BSA) was dissolved in the permeabilization buffer. Prior to commencing the experiment, cells were seeded into a 24-well plate at a concentration of 1×10^5 cells/ml and incubated undisturbed for 48 hours. The cell medium was then replaced with 500 μ l of the BrdU labeling solution, which contained 10 μ M BrdU. The cells were subsequently incubated at 37 $^{\circ}$ C with 5% CO₂, as required. After removing the labeling solution, the cells were washed three times for two minutes each with phosphate-buffered saline (PBS). Following the PBS washes, 500 μ l of a 4% formaldehyde solution in PBS was added to the culture. The cells were incubated for 15 minutes at 37 $^{\circ}$ C with 5% CO₂, after which they were washed three times for two minutes each with PBS. Once the PBS was removed, 500 μ l of Triton X-100 permeabilization buffer was added. The cells were then incubated at room temperature for 20 minutes, after which the Triton X-100 permeabilization buffer was removed and 500 μ l of 2N hydrochloric acid (HCl) was added. The cells were cultured for an additional 30 minutes at room temperature. After the removal of the 2N HCl, three 2-minute washes with Triton X-100 permeabilization buffer were performed. Subsequently, 500 μ l of the blocking

buffer was added, and the cells were incubated at room temperature for 30 minutes. To this culture, 500 μ l of blocking buffer containing the anti-BrdU primary antibody (sc-32323; Santa Cruz Biotechnology, Texas, USA) at a 1:200 dilution was added. Following an overnight incubation at 4 °C, the cells were washed three times for five minutes each with Triton X-100 permeabilization buffer. The cells were then incubated at room temperature for one hour after the addition of secondary antibodies (1:500 dilution) and DAPI (1:1000 dilution). The culture was subsequently washed three times for five minutes each with Triton X-100 permeabilization buffer before the addition of PBS. Finally, the cells were examined using an EVOS™ FL Auto 2 Imaging System (Invitrogen, Thermo Fisher Scientific, Massachusetts, USA). The quantification of BrdU⁺ cells was conducted by counting from 5 to 10 random microscope fields, including more than 4,000 nuclei for each group. Cell counting was automated using ImageJ software (National Center for Biotechnology Information, Bethesda, MD, USA).

Cell cycle analysis

In this study, JHH-4 cells were harvested and subsequently centrifuged at 400 g for 5 minutes. Following centrifugation, the cells were washed twice with cold PBS. To fix the cells, they were resuspended in 70% ice-cold ethanol and incubated overnight at -20 °C. Subsequently, the fixed cells were centrifuged at 600 g for 2 minutes, washed twice with 1% FBS in PBS, and resuspended in a dye mixture containing 100 μ g/mL RNase A (Thermo Scientific, Carlsbad, CA, United States; Cat

#EN0531) and 50 $\mu\text{g}/\text{mL}$ Propidium Iodide (Thermo Scientific, Carlsbad, CA, United States; Cat #P1304MP) in PBS. The cells were stained overnight at 4 °C and then subjected to DNA content analysis using the MACSQuant® X Flow Cytometer (Miltenyi Biotec, Gaithersburg, MD, USA). Flow cytometry data were subsequently analyzed and processed using FlowJo software (ver. 10.4, BD Biosciences Systems, San Diego, CA, USA) to differentiate the cells into G0/G1, S, and G2/M phases.

qRT-PCR analysis for candidate target proteins expression

Total RNAs from three cancer cell lines (HepG2, JHH-4, and SNU-449) were extracted using the GenUP™ Total RNA Kit (Biotechrabbit, Berlin, Germany) following the manufacturer's protocol. The RNAs were then reverse transcribed into cDNA for a duration of 45 minutes at 46 °C, utilizing the iScript™ Reverse Transcription Supermix (Bio-Rad, US), followed by heat inactivation for 1 minute at 95 °C. The resulting cDNA mixture was diluted fivefold with nuclease-free water. The qPCR reaction mixture, of a 10 μl final volume, contained 2.5 μl of 4X CAPITAL™ qPCR Probe Master Mix (Biotechrabbit, Berlin, Germany), 0.25 μl of each 10 μM primer, and 6 μl of nuclease-free water. The qPCR conditions consisted of an initial denaturation step at 95 °C for 10 minutes, followed by 40 cycles of denaturation at 95 °C for 15 seconds, and annealing/extension at 60 °C for 1 minute. All qPCR reactions were performed using a Life Technologies QuantStudio™ 3 real-time PCR system. The sequences of primers used in this step are shown in Table 5.

Table 5 Primer's sequence used for miRNA target expression analysis.

mRNA name	Forward primer (5' → 3')	Reverse primer (5' → 3')
RPL19	GCTCTTTCCTTTCGCTGCT	CATTGGTCTCATTGGGGTCT
CDK6	GAGAGCCGACTGCACTC	CAGAATCATTGCACCTGAGG

Dual luciferase assay

The first step involves cloning the 3' UTR sequences into the pmiRGLO vector using SacI and XhoI restriction sites and the hsa-miR-885-5p sequence into the pSilencer 3.0-H1 vector using BamHI and HindIII restriction sites. Then we transfected the 1×10^4 HEK293FT cell lines with a renilla-firefly plasmid and hsa-miR-885-5p using jetPRIME[®] transfection reagent, according to the manufacturer's protocol. This study utilized three groups of pmiRGLO plasmids: the first group lacked 3' UTR inserts of the target mRNA, the second group contained the 3' UTR of the target mRNA downstream to firefly luciferase, and the final group included mutant 3' UTRs of the target mRNA. To assess the activity of firefly luciferase, we performed the Dual-Luciferase[®] Reporter Assay Kit (Promega, Wisconsin, USA). Initially, the cells were lysed using 20 μ l of Passive Lysis Buffer (PLB) and agitated for 15 minutes at room temperature. Subsequently, 50 μ l of LAR II was added to each well, and luminescence was measured to observe firefly luciferase activity utilizing the BioTek[™] Synergy[™] HTX Multi-Mode Microplate Reader (Biotek, Thermo Fisher Scientific, Vermont, USA). Finally, Stop&Glo[®] reagent was introduced to terminate firefly luciferase activity, followed by measurement of renilla luciferase activity.

Protein extraction

The HCC cells (HepG2 and JHH-4) were subjected to lysis using 0.25% trypsin for a duration of 3 minutes. Subsequently, the resulting cell lysate was neutralized and transferred to a 1.5-ml microcentrifuge tube. The cell lysate was then subjected to centrifugation at 130 g for 2 minutes, after which the supernatant was carefully decanted. To each 1.5-ml microcentrifuge tube containing the cell lysate, 200-300 μ l of 1X protease inhibitor in RIPA buffer was added, ensuring thorough mixing and resuspension. The protein lysates were subsequently stored at -80°C until further use.

Bradford assay for determining protein concentration

To prepare the sample solution, the protein lysate underwent centrifugation at 16,000 g for 3 minutes, and subsequently, the supernatant was transferred into a new tube. For standardization, BSA standard (1 mg/ml) was diluted with DI water at various amounts: 0, 1, 2, 4, 8, and 10 μ g. Pipet 10 μ l of each standard and 5-fold diluted sample solution, along with their duplicates, into separate wells of a microtiter plate. Following this, 200 μ l of a 5-fold diluted dye reagent was added to each well, and the plate was incubated at room temperature for 5 minutes. The absorbance of the solutions was measured at 595 nm using a BioTek™ Synergy™ HTX Multi-Mode Microplate Reader (Biotek, Thermo Fisher Scientific, Vermont, USA). By subtracting the absorbance of the protein from the absorbance of the standard at 0 mg/ml, the protein concentration was calculated employing a linear trending

equation. Subsequently, 5X Laemmli buffer was combined with the protein to attain the desired final concentration and volume, and the mixture was boiled for 5 minutes at 100 °C.

Western blot

First, gel electrophoresis is used to separate the sample's proteins by size. A 12% resolving gel solution was prepared by combining the following components: 2.8 ml of deionized (DI) water, 1.5 ml of a 40% acrylamide/Bis solution, 628 µl of a 1.5 M Tris-HCl solution at pH 8.8, 50 µl of a 10% SDS solution, 37.3 µl of a 10% APS solution, and 2.67 µl of TEMED. The resulting resolving gel solution was placed between a glass plate and a short plate. For the stacking gel solution, the following components were mixed: 1 ml of DI water, 154 µl of a 40% acrylamide/Bis solution, 400 µl of a 0.5 M Tris-HCl solution at pH 6.8, 16 µl of a 10% SDS solution, 20 µl of a 10% APS solution, and 2 µl of TEMED. This mixture was used to create a 3.75% stacking gel solution, which was placed over the resolving gel solution. The gel comb was inserted into the solution. After the gel set, the gel was transferred to a tank and filled with 1X running buffer. The proteins were loaded into separate wells, and an initial voltage of 70V was applied for 15 minutes to line up the proteins in the gel. Subsequently, the voltage was increased to 130V and maintained for 80 minutes using the PowerPac™ Basic Power Supply (Bio-Rad, Hercules, California). To transfer the proteins from the gel to a nitrocellulose membrane, a voltage of 20V was applied for 30 minutes using the PowerPac™ HC High Current Power Supply (Bio-Rad,

Hercules, California). The gel was discarded, and the nitrocellulose membrane was incubated with BlockPRO™ 1 MIN Protein-Free Blocking Buffer (Visual Protein, Taipei, Taiwan) at room temperature on a shaker for a duration of 2 hours. Following the incubation period, a specific primary antibody (Anti-CDK6, sc-7961, Santa Cruz) was added to the blocking buffer at a ratio of 1:1,000 and incubated overnight at 4°C on a shaker. The nitrocellulose membrane was washed three times with 0.05% tween in 1X TBS, with each wash lasting for 10 minutes. Next, a secondary antibody (Anti-mouse IgG, HRP-linked Antibody #7076) in a ratio of 1:5,000 was added to the BlockPRO™ 1 MIN Protein-Free Blocking Buffer at room temperature on a shaker for 1 hour. The nitrocellulose membrane was washed three times with 0.05% tween in 1X TBS, with each wash lasting for 10 minutes. To enhance visualization, ECL detection reagents (Amersham™, Cytiva, Massachusetts, USA) were applied to the nitrocellulose membrane, and the membrane was visualized using a UVP ChemStudio (Analytik Jena, Germany). The resulting bands were analyzed using ImageJ software.

Sample preparation for RNA-Seq

Mir-885-transfected JHH-4 cells were cultured in 24-well plates until they reached confluence. Subsequently, the cells were harvested for RNA extraction utilizing the RNeasy Mini Kit (Qiagen), following the manufacturer's protocol, which included on-column DNA digestion. A minimum of 3 µg of total RNA was loaded into GenTegra-RNA 0.5 mL screw-cap microtubes (GenTegra) and subjected to vacuum treatment until complete desiccation. RNA integrity was assessed using the Agilent

Bioanalyzer 2100 system (Agilent Technologies). The NEBNext[®] Ultra[™] RNA Library Prep Kit for Illumina[®] (New England Biolabs, Massachusetts, USA) was employed for library preparation, utilizing 1 µg of total RNA with a RIN value exceeding 7. Subsequently, the library underwent sequencing using the NovaSeq 6000 System (Illumina). The NGS service and data analysis were conducted by Biomarker Technologies (BMKGene). Subsequent data analysis was performed to identify potential candidate target proteins.

GO term and pathway analysis

The g:Profiler web tool was employed for Gene Ontology (GO) term and pathway analysis [112]. To achieve this, all genes that exhibited downregulation in the RNA-seq analysis were subjected to functional analysis. The statistical domain scope was restricted to "only annotated genes". Statistical significance thresholds were determined using the g:SCS algorithm, and p-values lower than 0.05 were deemed statistically significant.

Statistical analysis

Data analyses were performed using GraphPad Prism 9 (GraphPad Software, Inc., San Diego, CA) to execute non-paired t-tests, Kaplan-Meier survival analysis, and One-way ANOVA. A p value <0.05 was considered statistically significant.

Chapter 6 Results

MicroRNA expression profile analysis identified hsa-miR-885-5p as a candidate miRNA

In the GEO database, the expression profiles of miRNAs obtained from GSE147889 indicate that a total of 100 miRNAs exhibited significant downregulation when the logFC was less than -0.5 and the adjusted p-value was below 0.05. The results obtained from the TCGA database revealed that 233 miRNAs were downregulated when comparing HCC tissue to normal tissue, while 66 miRNAs were found to be downregulated when comparing stage III HCC to stage I HCC. After cross-referencing the miRNAs from both databases, a set of nine miRNAs were identified as commonly downregulated (Figs. 8a and 8b). Next, in order to refine the list of miRNAs, a 5-year survival analysis was conducted in the TCGA database, focusing on miRNAs with high expression levels (threshold set at the 80th percentile). Among these nine miRNAs, it was observed that higher expression of hsa-miR-99a-5p, hsa-miR-99a-5p, hsa-miR-122-3p, hsa-miR-139-5p, and hsa-miR-885-5p was positively correlated with a higher 5-year survival rate (Figs. 8b, S1). In this study, the emphasis was placed on investigating the predominant forms of miRNAs; therefore, any non-predominant forms were excluded (Fig. 8b). In order to identify the potential candidate miRNA, we considered the number of studies of these miRNAs related to HCC. Hsa-miR-885-5p emerged as a particularly compelling candidate miRNA due to

the limited existing studies. The expression profiles of hsa-miR-885-5p, along with the corresponding survival curve, are presented in Figures 8c-f.

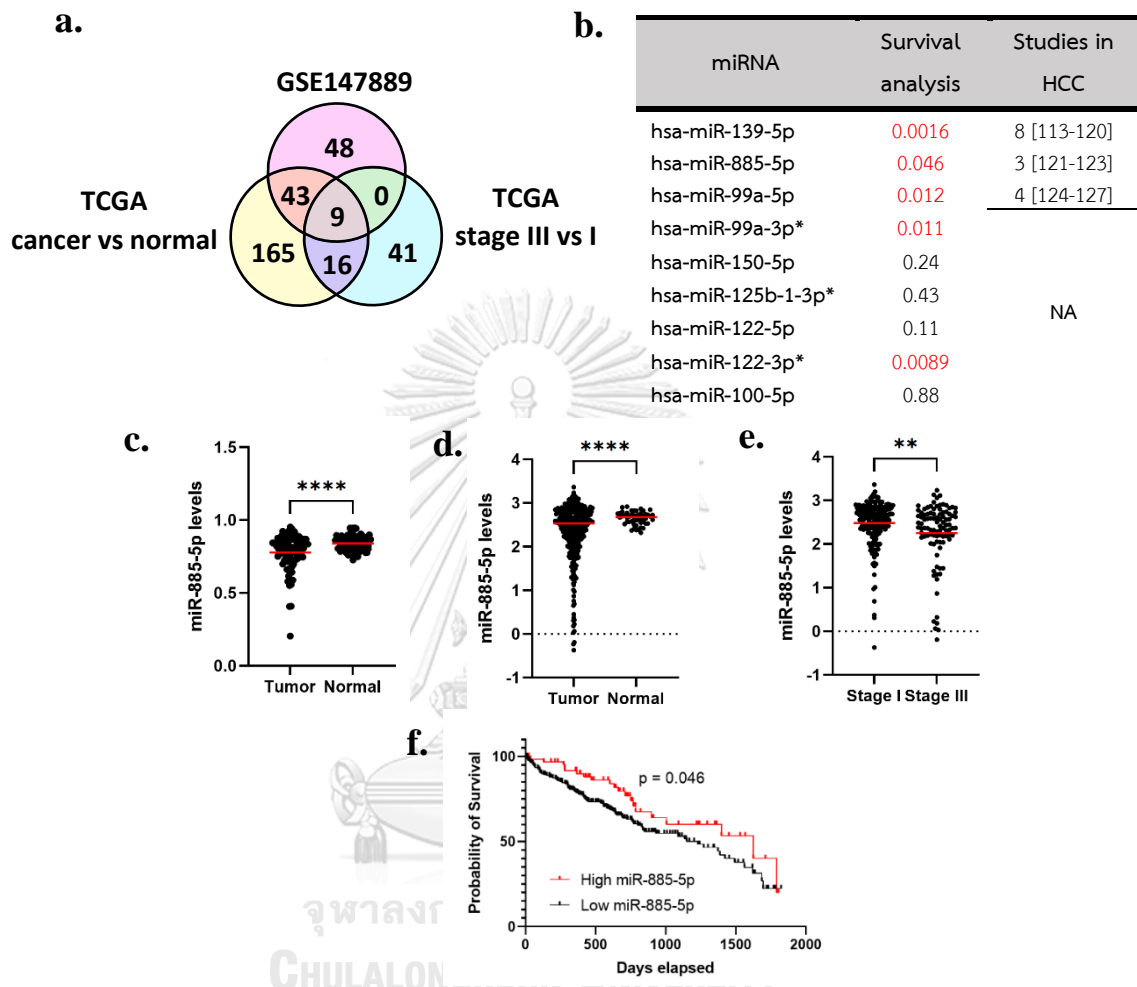


Fig. 8 Preliminary analysis of downregulated miRNAs in HCC.(a) Venn diagram of downregulated miRNAs from the GEO and TCGA databases. (b) List of commonly downregulated miRNAs. An asterisk indicates non-predominant forms of miRNAs. The red font indicates no association between miRNA expression levels and survival rates ($p > 0.05$). (c) Expression level of hsa-miR-885-5p between normal and tumor tissue in GSE147889. (d) Expression level of hsa-miR-885-5p between normal and tumor tissue in the TCGA database. (e) Expression level of hsa-miR-885-5p between stage I and stage III tumors in the TCGA database. Red lines indicate the mean. (f) Kaplan-Meier curves of hsa-miR-885-5p. Student's t-test with Welch's correction or Kaplan-

Meier survival analysis; ** = $p < 0.01$ and **** = $p < 0.0001$ **Hsa-miR-885-5p is highly downregulated in cancer cell**

To determine the role of hsa-miR-885-5p in association with HCC, we conducted an analysis of hsa-miR-885-5p expression profiles in HCC cell lines in comparison to a normal hepatocyte cell line, employing the RT-qPCR technique. As depicted in Figure 9, the findings demonstrate a notable downregulation of hsa-miR-885-5p in HCC cell lines (HepG2, JHH-4, and SNU-449) when contrasted with THLE-2, the selected normal hepatocyte cell line. The expression profiles indicate the most significant downregulation of hsa-miR-885-5p in the JHH-4 cell line, exhibiting an 82.73-fold decrease in comparison to THLE-2, followed by HepG2 and SNU-449 cell lines, which showed fold changes of 6.47 and 1.51, respectively. These observations strongly suggest that hsa-miR-885-5p may exert a pivotal role in the development of HCC.

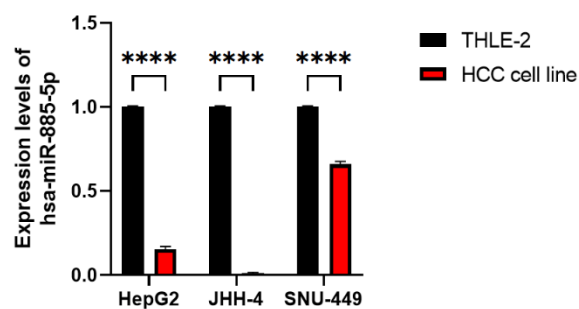


Fig. 9 Expression level of hsa-miR-885-5p in HCC cell lines (HepG2, JHH-4, and SNU-449). Data are presented as mean \pm SD and expressed relative to those of THLE-2 (set as 1.0). U6 was used as a housekeeping gene. N = 3 replicates per group from at least two independent experiments. Student's t-test; **** = $p < 0.0001$

Hsa-miR-885-5p suppresses the growth of HCC cells *in vitro*

To further validate the functional role of hsa-miR-885-5p in HCC progression, we established HCC cell lines expressing hsa-miR-885. The gel electrophoresis analysis of the PCR product of the pri-miRNA of hsa-miR-885, along with its 200 bps upstream and downstream sequences (Fig. 10a), indicates a successful amplification. The expected product size, resulting from the primer used in this step, should yield 649 bps. Furthermore, Sanger sequencing analysis (Fig. S2) serves to confirm the successful construction of the hsa-miR-885 plasmid. Following the selection process using puromycin until the disappearance of the negative control (Fig. 10b), we verified the overexpression of hsa-miR-885-5p through RT-qPCR. The expression levels of hsa-miR-885-5p were found to be significantly upregulated in hsa-miR-885-overexpressing cell lines, exhibiting 6.17-fold, 58.2-fold, and 49.64-fold increases in HepG2, JHH-4, and SNU-449, respectively (Fig. 10c-e). These findings indicate successful delivery and expression of hsa-miR-885. Furthermore, HCC cells carrying hsa-miR-885 demonstrated a notable reduction in cell proliferation compared to the control, as determined by the MTT assay (Fig. 10f-h). The MTT assay determines the conversion of yellow MTT to purple formazan crystals by metabolically active cells or viable cells, which can be observed using a spectrophotometer. The higher conversion of MTT to formazan, resulting in high absorbance at 570 nm, indicates a higher number of cells. This outcome further supports the inhibitory role of hsa-miR-885-5p in HCC cell proliferation.

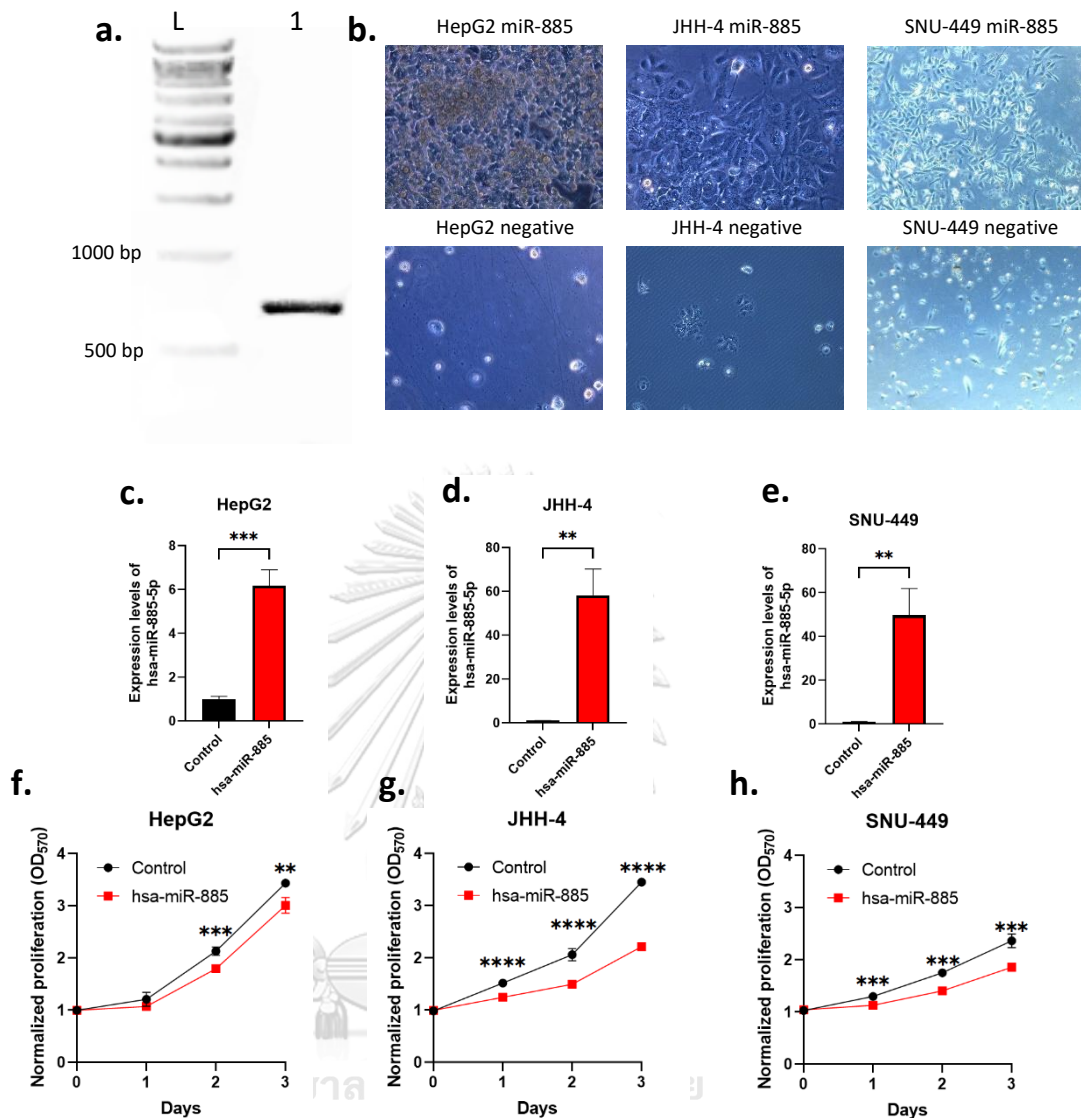


Fig. 10 Hsa-miR-885-3p attenuates cells growth in vitro. (a) Gel electrophoresis of the PCR product of pri-miRNA-885. The target-specific band size is around 649 bp. Lane L 1Kb DNA ladder; Lane 1 PCR product (b) Cell viability after puromycin selection. (c-e) qPCR-based quantification of relative expression of hsa-miR-885-5p in hsa-miR-885-overexpressed HCC cell lines compared with control. (f-h) Proliferation rate of HCC cell lines (HepG2, JHH-4, and SNU-449, respectively). Data are presented as mean \pm SD and expressed relative to those of control (set as 1.0) for qPCR analysis. U6 was used as a housekeeping gene. $N \geq 3$ replicates per group. Student's t-test; ** = $p < 0.01$, *** = $p < 0.001$, and **** = $p < 0.0001$

Hsa-miR-885-5p inhibits the G1/S transition of HCC cells

As MTT assays indicate a proliferative inhibitory effect of hsa-miR-885-5p, we suspect that hsa-miR-885-5p can prevent cell cycle progression, especially G1/S transition, which plays an important role for cell proliferation. To confirm this hypothesis, we analyzed cells in S phase using the BrdU incorporation assay. The BrdU assay is a method used to detect the incorporation of BrdU, a thymidine analog, into newly synthesized DNA in replicating cells. During the assay, cells are exposed to BrdU, which is incorporated into the DNA during the S phase of the cell cycle. The incorporated BrdU can then be detected using anti-BrdU antibodies, allowing researchers to determine the proportion of cells that are actively replicating their DNA [128]. Thus, the BrdU assay can be used to determine if there is a decrease in the proportion of cells in S phase, indicating that cells are being arrested in G1 phase and not progressing to S phase. As shown in Figures 11-13, the results suggested that hsa-miR-885-5p could decrease G1 phase progression in HepG2, JHH-4, and SNU-449, respectively, additionally verifying the antiproliferative effect of hsa-miR-885-5p. Furthermore, in order to provide additional evidence supporting the inhibition of the G1/S transition by hsa-miR-885-5p, a comprehensive analysis of the cell cycle was conducted. The findings obtained from the cell cycle analysis, as depicted in Figure 14, clearly demonstrated that hsa-miR-885-5p elicited G1 arrest, resulting in an elevated population of cells in the G1 phase while simultaneously decreasing the number of cells in the S and G2/M phases.

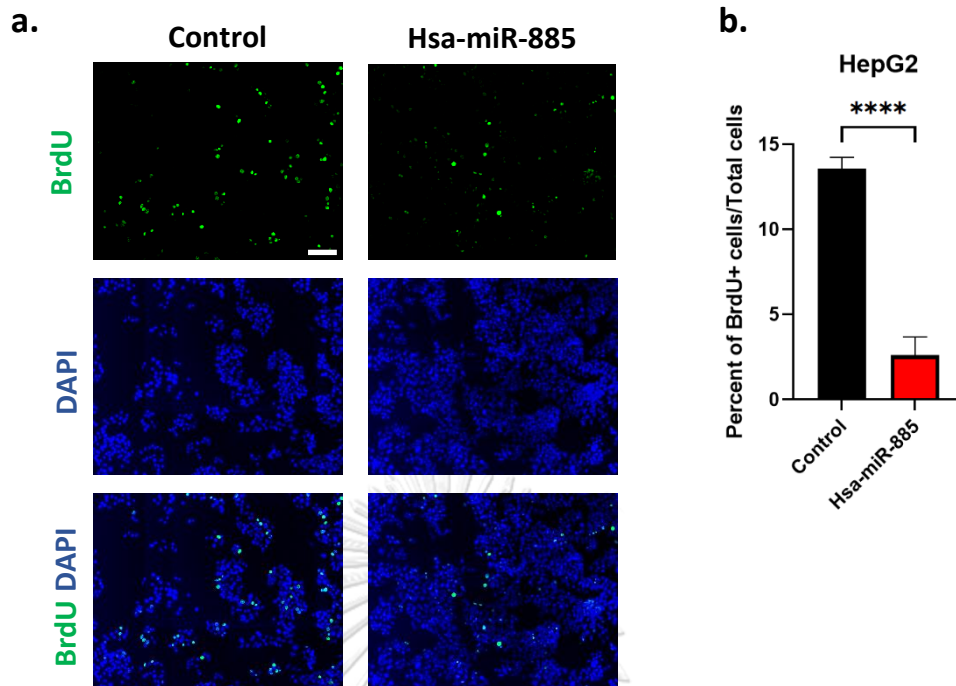


Fig. 11 BrdU incorporation assay of HepG2.(a) Representative fields of cells are shown stained with anti-BrdU (top panels) or DAPI (middle panels), with merged images shown in the bottom panels. (b) Quantitative data showing the percentage of BrdU-positive cells. Scale bars, 100 μ m. Data are presented as mean \pm SD. N > 3 replicates per group. Quantification of BrdU⁺ cells were performed from 5 random microscope fields, including > 6,000 nuclei. DAPI: 4',6-diamidino-2-phenylindole. Student's t-test; **** = $p < 0.0001$

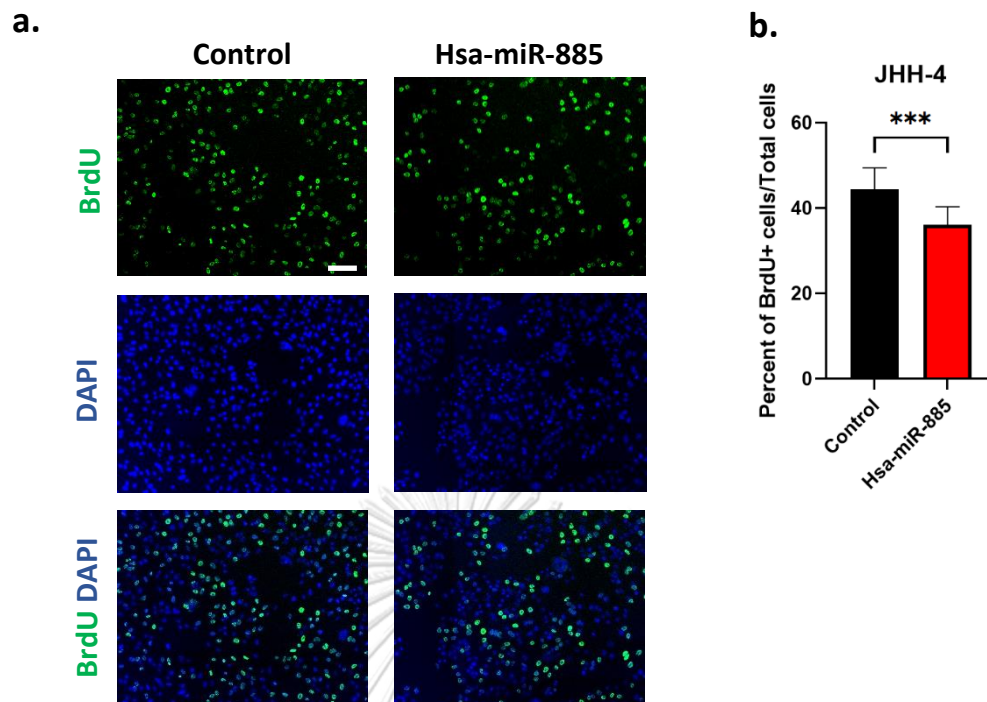


Fig. 12 BrdU incorporation assay of JHH-4.(a) Representative fields of cells are shown stained with anti-BrdU (top panels) or DAPI (middle panels), with merged images shown in the bottom panels. (b) Quantitative data showing the percentage of BrdU-positive cells. Scale bars, 100 μ m. Data are presented as mean \pm SD. N > 3 replicates per group. Quantification of BrdU⁺ cells were performed from 10 random microscope fields, including > 6,000 nuclei. DAPI: 4',6-diamidino-2-phenylindole. Student's t-test; *** = $p < 0.001$

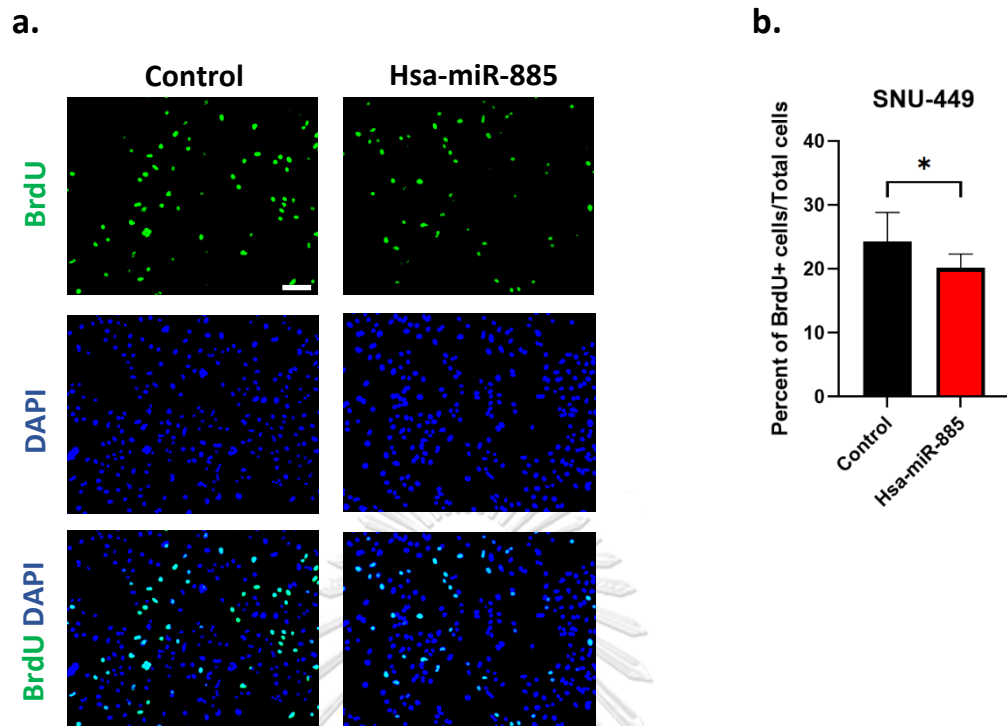


Fig. 13 BrdU incorporation assay of SNU-449.(a) Representative fields of cells are shown stained with anti-BrdU (top panels) or DAPI (middle panels), with merged images shown in the bottom panels. (b) Quantitative data showing the percentage of BrdU-positive cells. Scale bars, 100 μ m. Data are presented as mean \pm SD. N > 3 replicates per group. Quantification of BrdU⁺ cells were performed from 5 random microscope fields, including > 4,000 nuclei. DAPI: 4',6-diamidino-2-phenylindole. Student's t-test; * = $p < 0.05$

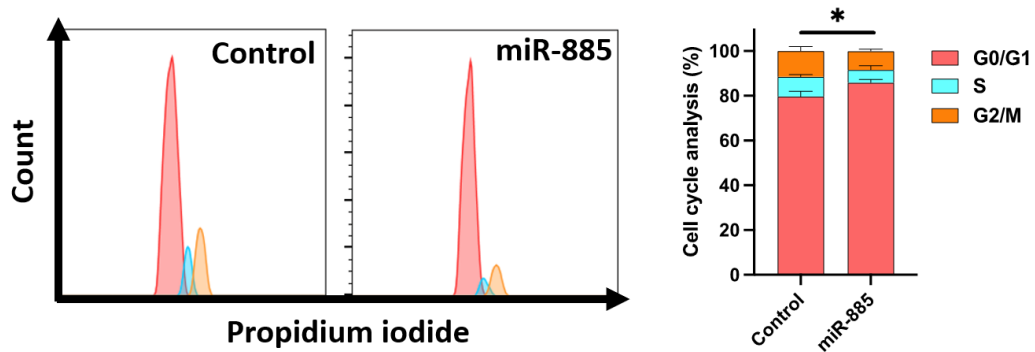


Fig. 14 Cell cycle analysis of JHH-4 cells. N > 3 replicates per. Student's t-test; * = $p < 0.05$

***CDK6* is predicted as a hsa-miR-885-5p target**

To identify the potential target of hsa-miR-885-5p, miRNA target prediction was performed using TargetScan. Given the previous discovery that hsa-miR-885-5p effectively suppresses the G1/S transition, the focus was on predicted targets associated with this cellular phase transition. Out of a total of 3,082 predicted mRNA targets, 32 were found to be specifically linked to the progression of cells from G1 to S phase. These G1/S predicted targets of hsa-miR-885-5p are presented in Table 6. To narrow down the search for a single potential hsa-miR-885-5p target mRNA, we excluded any mRNA targets with a Context++ score percentile below 60. The Context++ score is a metric utilized by TargetScan to estimate the likelihood of miRNA targeting a particular site within an mRNA. The context++ score percentile represents a transformed value of the context++ score, facilitating the interpretation of the results. A higher context++ score percentile suggests a greater probability that the predicted target site is indeed a true target of the miRNA compared to other sites. Subsequently, we conducted an analysis to examine the correlation between the expression levels of hsa-miR-885-5p and mRNAs. Notably, Table 6 and Fig. S3 illustrate that *CDK6* exhibits the highest negative correlation with hsa-miR-885-5p. This observation strongly implies that *CDK6* could be a specific target of hsa-miR-885-5p, thus warranting further investigation.

Table 6 The lists of G1/S predicted targets of hsa-miR-885-5p.

mRNA	Context++ score percentile	Correlation coefficient	p value
CDK6	62	-0.45	3.9e-20
PPP2R1A	87	-0.3	3.3e-9
CDK7	94	-0.27	2.8e-7
PSMD11	83	-0.26	5.2e-7
PPP2R2A	78	-0.25	1.1e-6
DYRK1A	67	-0.24	2.3e-6
ORC2	94	-0.23	6.3e-6
CDKN2C	61	-0.21	4.3e-5
UBA52	78	-0.2	1.5e-4
RBBP4	83	-0.18	5.5e-4
PPP2CA	67	-0.18	4.7e-4
CDKN2B	62	-0.18	6.8e-4
ORC1	76	-0.17	7.7e-4
PSMA1	91	-0.14	8.8e-3
SKP1	78	-0.14	7.6e-3
PSMF1	84	-0.12	0.027
CCNA2	82	-0.12	0.025
RPA3	74	-0.12	0.021
RPA4	84	-0.11	0.04
PSMC4	93	-0.03	0.53
LIN52	80	-0.03	0.52
E2F2	55		
MYC	35		
CCND1	35	NA	
PSMB9	35		
PSMD1	35		

mRNA	Context++ score percentile	Correlation coefficient	p value
PSMB5	35		
PSMD12	35		
E2F1	35		
ORC6	35		NA
RBL1	35		
CCNB1	35		

Hsa-miR-885-5p directly interacts with the 3'UTR of *CDK6* transcripts

The interaction between hsa-miR-885-5p and *CDK6* was further analyzed via a dual-luciferase assay in order to confirm the hypothesis that hsa-miR-885-5p possesses the ability to suppress *CDK6* expression. Initially, the dual-luciferase assay was validated using empty pSilencer as a positive control and Luc2 pSilencer as a negative control. The successful validation of the assay is depicted in Figure S4. The sequences of hsa-miR-885-5p, the wild-type 3' UTR of *CDK6*, and the mutant 3' UTR of *CDK6* are presented in Figure 15a. The findings indicate a direct targeting of *CDK6* by hsa-miR-885-5p, resulting in the suppression of its expression. Furthermore, when the 3' UTR of the *CDK6* sequence was mutated, hsa-miR-885-5p was rendered incapable of inhibiting *CDK6* expression (Fig. 15b).

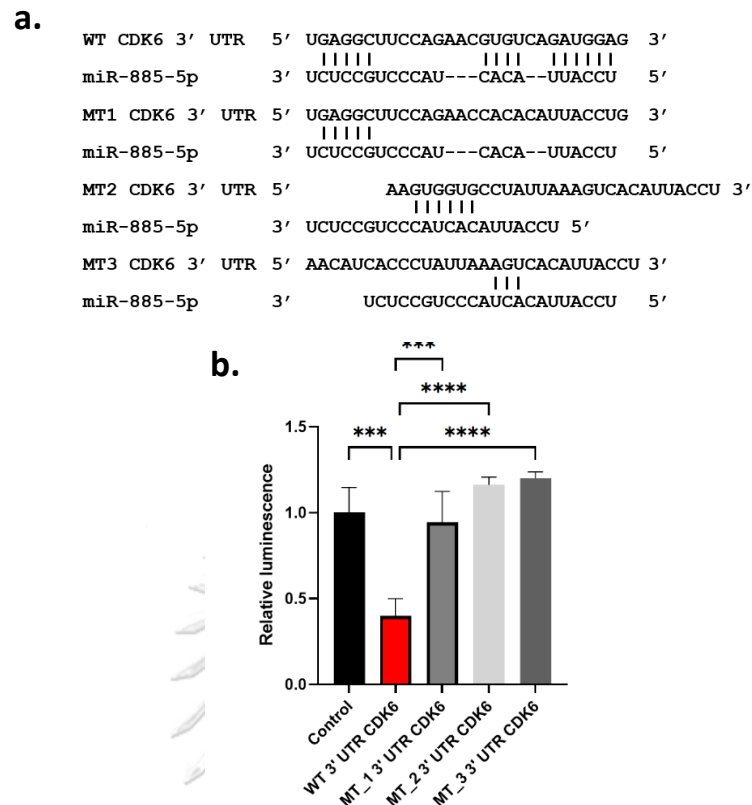


Fig. 15 CDK6 is a direct target of hsa-miR-885-5p.(a) Sequences of hsa-miR-885-5p, the wild-type (WT) 3' UTR of CDK6, and the mutant (MT) 3' UTR of CDK6. (b) Dual-luciferase reporter assay of MT1, MT2, and MT3, respectively. Data are presented as mean \pm SD and expressed relative to those of control (set as 1.0). N = 3 replicates per group. One-way ANOVA; *** = $p < 0.001$ and **** = $p < 0.0001$

CHULALONGKORN UNIVERSITY

Overexpression of hsa-miR-885-5p inhibits expression of CDK6

Considering the reduced rates of BrdU incorporation observed in cells overexpressing hsa-miR-885 (Figs. 11-13), the alterations in the population of cells within the G₀, S, and G₂/M phases (Fig. 14), and the identification of CDK6 as a specific target of hsa-miR-885-5p, a significant regulator involved in the G₁/S transition (Fig. 15), the hsa-miR-885-5p/CDK6 axis was further validated using qPCR and western blot techniques. It was determined that the overexpression of hsa-miR-

885 resulted in a notable reduction in CDK6 transcript levels across HCC cell lines (HepG2, JHH-4, and SNU-449) (Fig. 16a-c). The downregulation of CDK6 in cells overexpressing hsa-miR-885 was further confirmed at the protein level through Western blot analysis (Fig. 16d). Collectively, the hsa-miR-885-5p/CDK6 axis was proposed as a novel regulatory mechanism facilitating proliferation in HCC cells (Fig. 17).

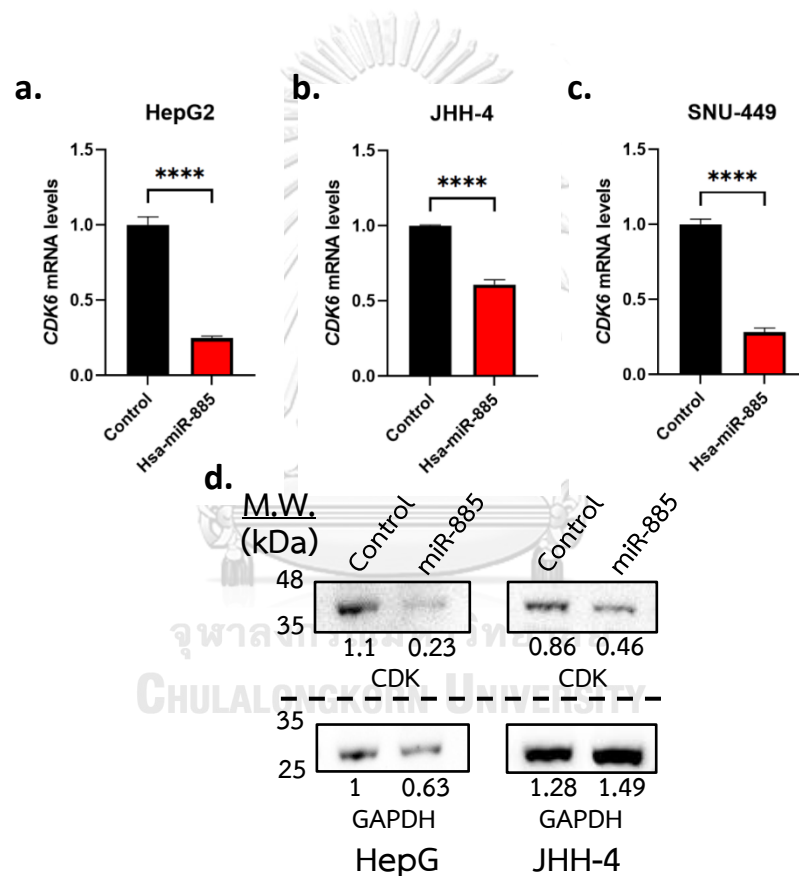


Fig. 16 Hsa-miR-885-5p inhibits expression of CDK6. (a) Expression levels of *CDK6* in HepG2. (b) Expression levels of *CDK6* in JHH-4. (c) Expression levels of *CDK6* in SNU-449. (d) Western blot of CDK6 in HCC cells (HepG2 and JHH-4). GAPDH used as a loading control. Data are presented as mean \pm SD and expressed relative to those of control (set as 1.0). RPL19 was used as a housekeeping gene. N = 3 replicates per group for qPCR analysis. Student's t-test; **** = $p < 0.0001$

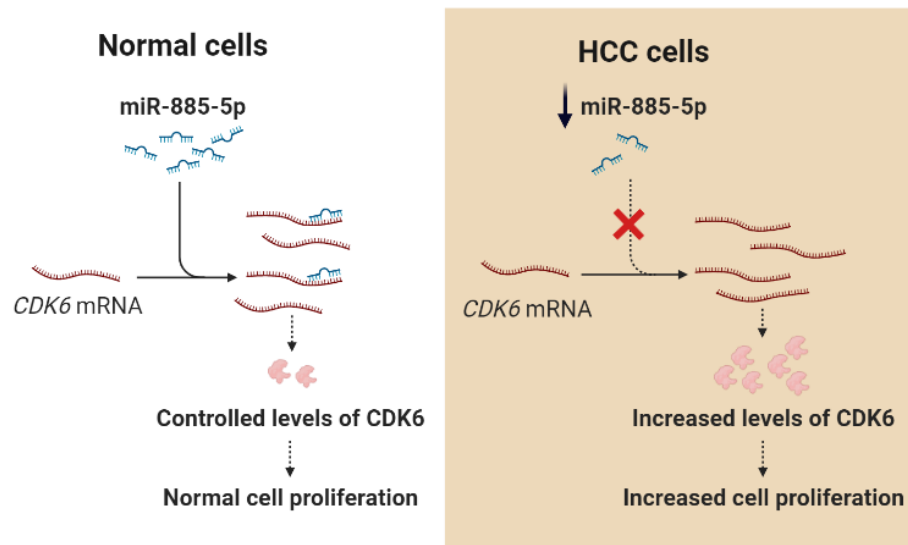


Fig. 17 Proposed mechanism of hsa-miR-885-5p in promoting proliferation of HCC cells via targeting *CDK6*. In normal cells, hsa-miR-885-5p negatively regulates the expression of *CDK6*. However, levels of hsa-miR-885-5p are suppressed in HCC cells, allowing upregulation of *CDK6* to drive the cell cycle and thus promote cell proliferation.

RNA-Seq analysis identified the G1/S transition as a potential pathway for hsa-miR-885-5p in HCC

In this work, the potential mRNA targets of hsa-miR-885-5p were unbiasedly identified using RNA-seq in the JHH-4 cell line, which exhibits the highest expression of hsa-miR-885-5p among overexpressing cell lines. Among the 990 downregulated genes, a total of 797 annotated genes with $\log_2FC \leq -0.5$ were observed. To gain further insights into the function of these identified target genes, GO term, KEGG, and Reactome pathway analyses were conducted (Fig. 18). The results revealed a significant enrichment of genes involved in cell cycle processes, thereby providing additional evidence for the antiproliferative role of hsa-miR-885-5p. Notably, genes

associated with the G1/S transition, a critical step in cell growth, exhibited prominent representation.

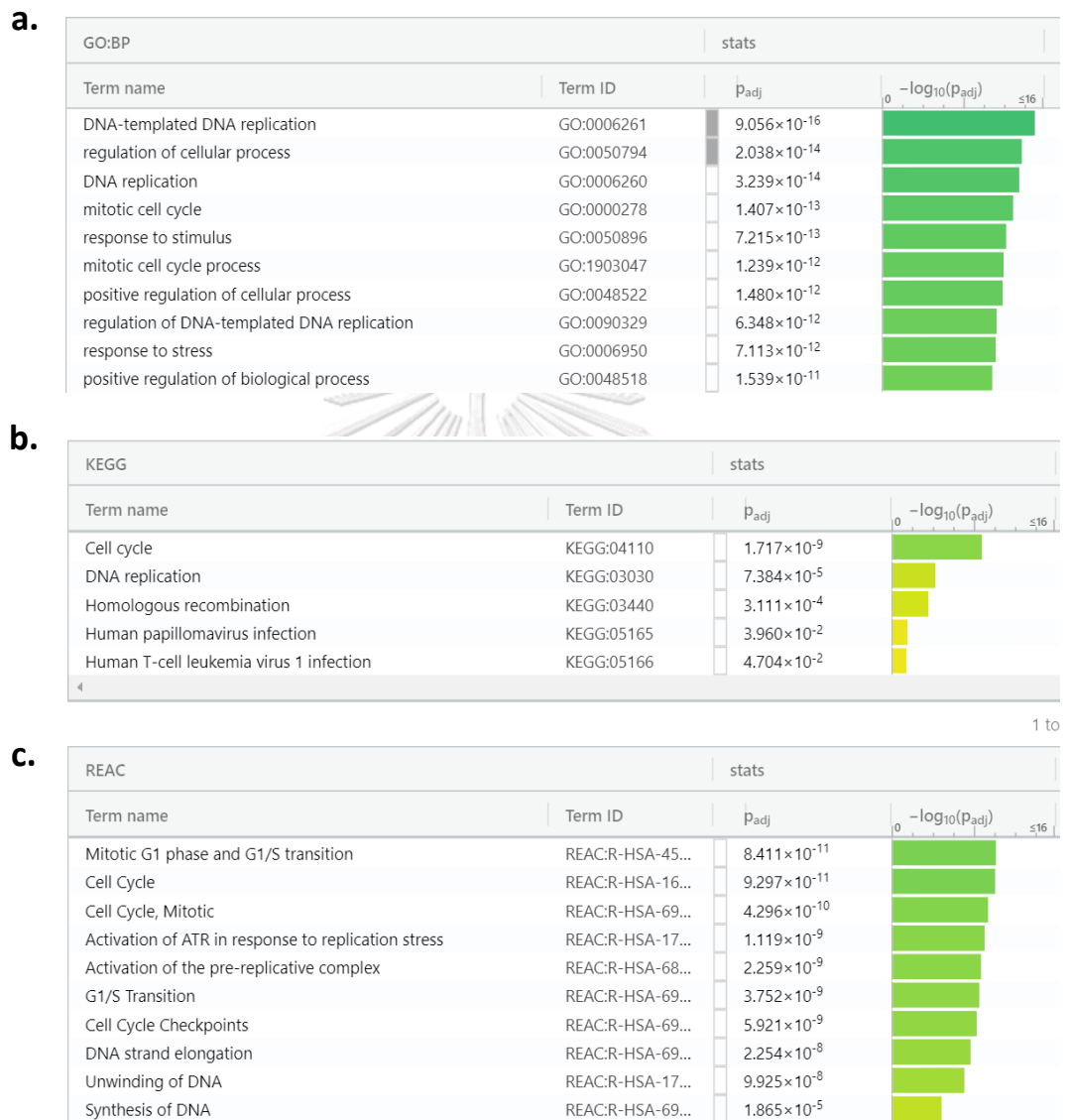


Fig. 18 GO term and pathway analysis of genes obtained from RNA-seq comparison between JHH-4 expressing hsa-miR-885 and control. (a) Biological Processes (BP) category of the GO term. (b) KEGG enrichment analysis. (c) Reactome pathway analysis.

As previously stated, it has been established that CDK6 possesses the ability to phosphorylate Rb family proteins and induce the dissociation of E2F from the inhibitory complex. In order to provide preliminary confirmation of this phenomenon, an analysis was conducted on the expression profiles of E2F target genes. From the RNA-seq data obtained, it was observed that a total of 50 mRNAs, known to be targets of E2F [129], exhibited downregulation in the hsa-miR-885-overexpressing JHH-4 samples (Fig. 19 and Table 7). This outcome serves to imply that hsa-miR-885-5p may exert a suppressive effect on the expression of CDK6, consequently impeding the phosphorylation of Rb and thereby preventing E2F from facilitating the expression of its target genes.

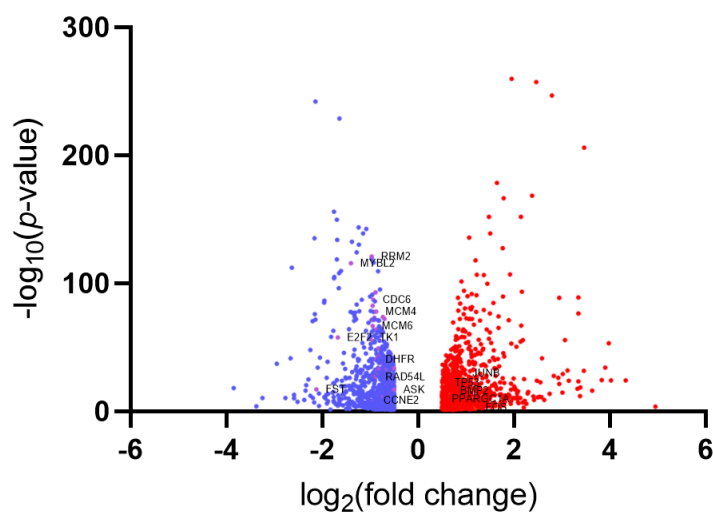


Fig. 19 Volcano plot displaying RNA-seq data. The plot illustrates all annotated genes exhibiting a log₂ fold change (log₂FC) exceeding |0.5| and a p-value greater than 0.05. Downregulated target genes of E2F are indicated by purple dots. Some gene names are provided within the figure.

Table 7 Lists of mRNAs targeted by E2F that are downregulated in RNA-seq and their functions

mRNA	Function
CCND3	G1
JUN	
CCNE2	
CDC25A	
CDK2	
E2F1	G1/S
E2F2	
MYBL2	
TK1	
AURKB	
CCNA2	
CDC20	S/G2
MKI67	
SMC4	
ASK	
CDC45	
CDC6	
CDC7	
DHFR	
MCM2	
MCM3	DNA synthesis and replication
MCM4	
MCM5	
MCM6	
MCM7	
ORC1	
PCNA	

mRNA	Function
POLA1	DNA synthesis and replication
POLA2	
POLD1	
RFC2	
RFC4	
RPA2	
RRM2	
TYMS	
BRCA1	Checkpoints
BRCA2	
CENPE	
CHEK1	
RAD51	
BARD1	DNA damage repair
MSH2	
RAD54L	
CASP3	Apoptosis
CASP7	
EZH2	Development
FST	Differentiation
PPARGC1B	
TGFA	

Chapter 7 Discussion and Conclusion

To identify potential miRNAs that exert a significant influence on HCC, an extensive bioinformatic analysis was employed to conduct a comparative examination of differential expression patterns between normal tissue and HCC tissue from both the GEO and TCGA databases, as well as between high-grade and low-grade tumor tissue solely from the TCGA database. Notably, our preliminary analysis unveiled nine downregulated miRNAs, namely hsa-miR-99a-3p, hsa-miR-99a-5p, hsa-miR-100-5p, hsa-miR-122-3p, hsa-miR-122-5p, hsa-miR-125b-1-3p, hsa-miR-139-5p, hsa-miR-150-5p, and hsa-miR-885-5p, which signify the potential of these miRNAs as tumor suppressors (Fig. 8b). In this study, pri-miRNAs were utilized as a platform for the overexpression of candidate miRNAs. Nonetheless, it is important to acknowledge that this platform possesses inherent limitations that hinder its ability to effectively express non-predominant miRNAs. Consequently, any non-predominant forms of miRNAs, including hsa-miR-99a-3p, hsa-miR-122-3p, and hsa-miR-125b-1-3p, were excluded from further analysis, as indicated by the asterisk symbol (Fig. 8b). Subsequently, survival analyses were conducted to explore the survival rate of patients based on the high or low expression levels of specific miRNAs. The survival analysis employed a 5-year cut-off, with expression levels exceeding the 80th percentile of all patients considered high expression, while expression levels falling below the 80th percentile denoted low expression. As a result, only hsa-miR-99a-5p,

hsa-miR-139-5p, and hsa-miR-885-5p demonstrated an association with improved survival rates among patients with high miRNA expression levels. To narrow down the selection to a single candidate miRNA, the miRNAs with the least comprehensive investigation in the context of HCC were chosen for further analysis. Consequently, hsa-miR-885-5p was selected to investigate its potential role in the progression of HCC. The expression profiles of hsa-miR-885-5p, as well as the results of the survival analysis, are clearly illustrated in Figures 8c-f.

In order to substantiate the hypothesis regarding the tumor-suppressive function of hsa-miR-885-5p in HCC, an assessment was conducted to confirm the downregulation of hsa-miR-885-5p within three distinct HCC cell lines (HepG2, JHH-4, and SNU-449) (Figure 9). A comparative analysis revealed that HCC cell lines exhibited a significantly lower expression level of hsa-miR-885-5p in comparison to the normal hepatocyte cell line (THLE-2). Consequently, these findings provide additional evidence supporting the anti-tumorigenic role of hsa-miR-885-5p.

Undoubtedly, hsa-miR-885-5p exerts a significant antiproliferative effect, manifesting in the suppression of cell proliferation in both MTT (Fig. 10f-h) and BrdU (Fig. 11-13) assays. The MTT assay serves as a robust means to determine cell proliferation by evaluating the conversion of MTT to formazan crystals through the metabolic activity of mitochondria in viable cells. This process can be observed using a spectrophotometer, wherein the presence of purple formazan indicates a heightened absorbance at 570 nm, thereby signifying a substantial number of viable

cells. Consequently, this outcome implies a heightened proliferation of cells. In parallel, BrdU incorporation assays play a pivotal role in discerning the proliferation rate of cells. By monitoring the incorporation of BrdU, a thymidine analog, into DNA strands during DNA synthesis, these assays effectively capture the cellular activity related to DNA replication and cell division. The BrdU assay becomes particularly insightful as DNA synthesis is characteristic of the S phase of the cell cycle, thereby providing valuable insights into potential G1 cell cycle arrest. The lower percentage of BrdU⁺ cells per total cell (DAPI⁺) observed in these assays serves as an indicative measure of the diminished proliferation rate of cells and the concurrent suppression of G1/S progression. To further substantiate the findings pertaining to the ability of hsa-miR-885-5p to induce G1 arrest, a comprehensive cell cycle analysis was performed. This analysis involved the utilization of propidium iodide, a fluorescent dye capable of intercalating with DNA, thereby enabling the quantification of DNA content within individual cells. The intensity of propidium iodide fluorescence is directly proportional to the DNA content present, facilitating the identification and characterization of cells in various stages of the cell cycle. Within this analysis, cells in the G1 phase are represented by a prominent peak, whereas cells in the G2/M phases are denoted by a peak with twice the intensity. Cells in the S phase are identifiable through a shoulder or broader peak positioned between the G1 and G2/M peaks. In light of the cell cycle analysis results (Fig. 14), it becomes increasingly evident that hsa-miR-885-5p plays a pivotal role in suppressing G1/S progression. In

conclusion, the collective evidence obtained from the MTT assay, BrdU incorporation assays, and cell cycle analysis unequivocally supports the notion that hsa-miR-885-5p exerts a potent antiproliferative influence by effectively inhibiting cell proliferation and impeding G1/S progression. In spite of the MTT results revealing that hsa-miR-885-5p possesses the capability to suppress the growth of HCC cell lines, the findings from the HepG2 experiment indicate only a marginal decrease in the proliferation rate. This discrepancy may be attributed to the relatively lower expression levels of hsa-miR-885-5p observed in the overexpressing cells. Consequently, it is imperative to consider implementing certain modifications to enhance the transfection efficiency of hsa-miR-885-5p in HepG2 cells, thereby ensuring more consistent outcomes across all cell lines. Furthermore, the BrdU results obtained from JHH-4 and SNU-449 exhibit only a slight decrease in the percentage of BrdU⁺ cells relative to the total cell count. Although statistically significant, these outcomes do not exhibit the same level of distinctness observed in the HepG2 results. To enhance the contrast between the control and hsa-miR-885-5p treatment groups, it is recommended to consider adjustments in the incubation times during the BrdU assay. By optimizing these incubation periods, it is possible to attain more discernible differences in the BrdU labeling patterns, enabling a more accurate assessment of the effect of hsa-miR-885-5p on cell proliferation in JHH-4 and SNU-449 cell lines. Additionally, to comprehensively evaluate the impact of hsa-miR-885-5p on cell cycle progression, it is crucial to conduct further experiments. Currently, only the results from the JHH-4

cell line are available, while data from the HepG2 and SNU-449 cell lines are lacking due to time constraints that prevented the execution of additional experiments. Performing additional experiments on these cell lines will provide a more comprehensive understanding of the influence of hsa-miR-885-5p on cell cycle dynamics and enable a more comprehensive analysis of its therapeutic potential in HCC treatment.

In accordance with our study, previous studies have also found that hsa-miR-885-5p can suppress tumors in many cancers, including neuroblastoma [130], gastric cancer [131], and HCC [123].

To gain a comprehensive understanding of the molecular mechanism underlying hsa-miR-885-5p, an extensive analysis was conducted, focusing on the identification of its potential target genes. The initial step involved retrieving a set of candidate target genes through a meticulous miRNA target prediction analysis. Subsequently, a stringent criterion was applied to narrow down the selection, concentrating solely on genes known to be associated with the crucial G1/S transition, as stipulated by the esteemed Reactome Pathway Database. From an initial pool of 149 genes, a refined list of 32 genes was generated, representing the potential targets of hsa-miR-885-5p as predicted by TargetScan. For further investigation, only those targets exhibiting a context++ score percentile exceeding 60 were deemed suitable for subsequent analysis. It is important to note that the context++ score percentile serves as an indicator of target favorability relative to

other potential targets, with higher percentiles signifying a greater likelihood of being a favorable target. Following the aforementioned selection criteria, an in-depth correlation analysis was performed between hsa-miR-885-5p and the predicted targets. Among the candidates, CDK6 emerged as a compelling candidate target, demonstrating a significant negative correlation with hsa-miR-885-5p, ascertained through meticulous bioinformatic analysis (Table 6). By adopting this rigorous analytical approach, we have successfully identified CDK6 as a potential target of hsa-miR-885-5p. This finding not only provides valuable insights into the molecular interactions involving hsa-miR-885-5p but also underscores the significance of CDK6 in the context of our research.

The hypothesis put forth in our research is substantiated by the employment of a dual luciferase assay, which has convincingly demonstrated our prediction regarding the targeting ability of hsa-miR-885-5p on *CDK6* (Fig. 15). Specifically, the assay reveals the direct binding capability of hsa-miR-885-5p to the wild-type 3' UTR of *CDK6*, leading to the suppression of firefly luciferase expression. Conversely, when utilizing mutant 3' UTRs of *CDK6*, it becomes evident that the interaction between hsa-miR-885-5p and the 3' UTR of *CDK6* is hindered. To further validate the regulatory effect of hsa-miR-885-5p on *CDK6*, we conducted additional analyses in the form of qPCR and western blot assays (Fig. 16). Remarkably, the qPCR analysis demonstrates reduced expression levels of *CDK6* in cells that overexpress hsa-miR-885-5p. This reduction strongly suggests that hsa-miR-885-5p induces the degradation

of *CDK6*. Moreover, the western blot assay effectively corroborates the degradation process of *CDK6* triggered by hsa-miR-885-5p, ultimately resulting in a lower expression level of the CDK6 protein. Additional investigations are warranted to enhance our understanding of the impact of hsa-miR-885-5p on CDK6 protein expression in SNU-449 cells, as this remains unexplored due to time limitations.

The RNA-seq analysis of downregulated genes in the presence of hsa-miR-885-5p overexpression provides compelling evidence of the crucial involvement of hsa-miR-885-5p in cell cycle processes, particularly the G1/S transition. This finding is strongly supported by the results obtained from Reactome pathway analysis, as depicted in Figure 18c. Consequently, it is highly plausible that hsa-miR-885-5p exerts a pivotal role as a negative regulator of the G1/S transition. Notably, the RNA-seq data reveal a substantial decrease in the expression of numerous E2F target genes in JHH-4 cells overexpressing hsa-miR-885-5p, as illustrated in Figure 19. These findings further corroborate the proposed mechanism of hsa-miR-885-5p's action, wherein it targets CDK6, a protein known to phosphorylate the Rb family proteins. Phosphorylated Rb proteins form inhibitory complexes with E2F, but upon phosphorylation by CDK6, they are released, thereby enabling E2F to promote the expression of its target genes. To definitively ascertain the functional role of hsa-miR-885-5p in the CDK6/Rb/E2F pathway, it is imperative to conduct a western blot assay. This assay should include the evaluation of pRb and tRb levels, along with the measurement of specific target proteins regulated by E2F. By performing this

experimental validation, we can establish with certainty whether hsa-miR-885-5p indeed functions through the CDK6/Rb/E2F axis.

Cell cycle processes are important for cancer. The aberration in cell cycle regulatory proteins has been found in virtually all human cancers [132]. The field of anticancer drug development has witnessed the emergence of numerous agents that target various components of the cell cycle, such as CDK4/6 selective inhibitors, which have demonstrated remarkable efficacy in treating cancer. Consequently, it becomes increasingly intriguing to delve deeper into exploring the therapeutic potential of hsa-miR-885-5p, a microRNA known to target CDK6, particularly in the context of HCC. In order to comprehensively elucidate the tumor-suppressing role of hsa-miR-885-5p, it is imperative to broaden the scope of investigation beyond solely examining cell proliferation. Multiple aspects of cancer biology should be taken into consideration, including but not limited to cell migration, invasion, and apoptosis. By investigating these additional facets, a more holistic understanding of the impact of hsa-miR-885-5p on HCC pathogenesis can be obtained. Furthermore, it is crucial to consider the potential benefits of co-treatment involving hsa-miR-885-5p and CDK6 inhibitors as a combined therapeutic approach. Assessing the effects of this dual strategy on tumor suppression holds great promise and may yield superior outcomes compared to employing either intervention in isolation.

In summary, HCC is a devastating disease with high incidence and mortality. In order to foster the development of efficacious therapeutic interventions for HCC, it is

imperative to gain a comprehensive understanding of the disease's underlying pathology. Our investigation has yielded noteworthy insights, revealing that the upregulation of hsa-miR-885-5p elicits a suppressive effect on cell proliferation and impedes the G1/S transition. Employing bioinformatic analysis techniques, we have successfully identified CDK6 as a promising candidate target of hsa-miR-885-5p. This prediction has been subsequently confirmed through luciferase assays, qPCR, and western blot analysis. Notably, there are certain anti-cancer medications that specifically target CDK6. By virtue of this knowledge, the targeting of CDK6 by hsa-miR-885-5p presents a potential avenue for the development of therapeutic strategies against cancer. Furthermore, through the utilization of RNA-seq, we have elucidated the role of hsa-miR-885-5p as a negatively regulatory microRNA during the G1/S transition, achieved by targeting numerous genes that are intricately involved in this process. Consequently, it is crucial to embark upon further investigation into the functional properties of hsa-miR-885-5p at this particular stage and explore the therapeutic potential of this microRNA. It is imperative to acknowledge that additional research endeavors should be undertaken in order to replicate and validate several outcomes derived from this study. Furthermore, to elucidate the mechanism underlying the action of hsa-miR-885-5p, it is essential to conduct western blot analysis of pRb and tRb, as well as other E2F targets. These comprehensive investigations will provide a more robust understanding of the mechanism by which hsa-miR-885-5p functions.

Appendix

Table S1 Primers used to amplify the pri-miRNA of hsa-miR-885.

Name	Sequence (5' → 3')
Forward pri-miR_885	GCTGAATTCAAACAGCAAGGCCTGGCTCC
Reverse pri-miR_885	CGAGGATCCGGGATGGAGGCTATTTCTGG

Table S2 Concentration of protein lysate and preparation of protein solution for western blot analysis.

Sample	Conc. ($\mu\text{g}/\mu\text{l}$)	Preparation of 100 μl protein solution (20 $\mu\text{g}/\mu\text{l}$)	
		Volume of protein	Volume of Laemmli
HepG2 control	59.81	33.44	66.56
HepG2 885	60.33	33.15	66.85
JHH4 control	61.89	32.32	67.68
JHH4 885	71.73	27.88	72.12

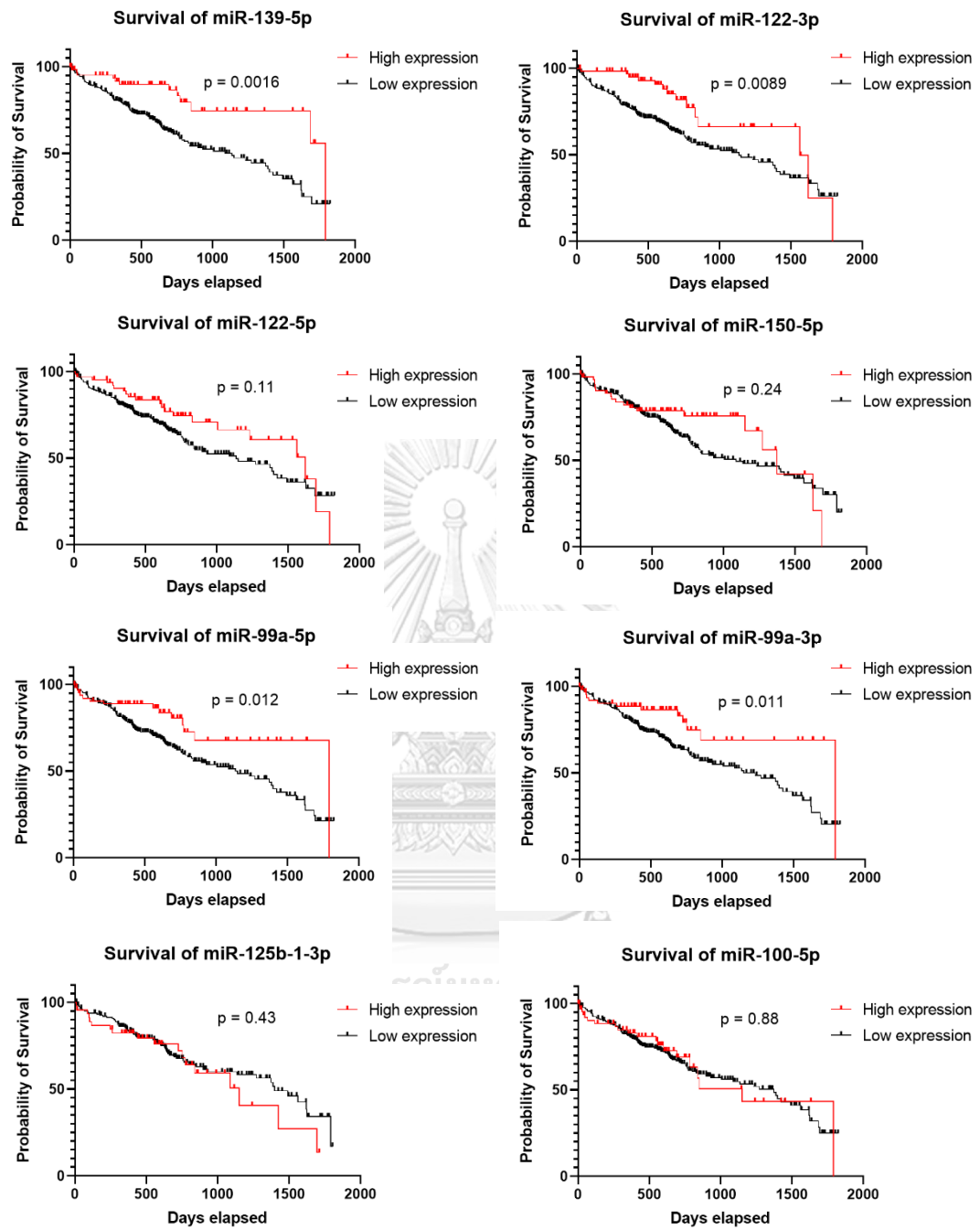


Fig. S1 Kaplan-Meier survival analysis of other miRNAs

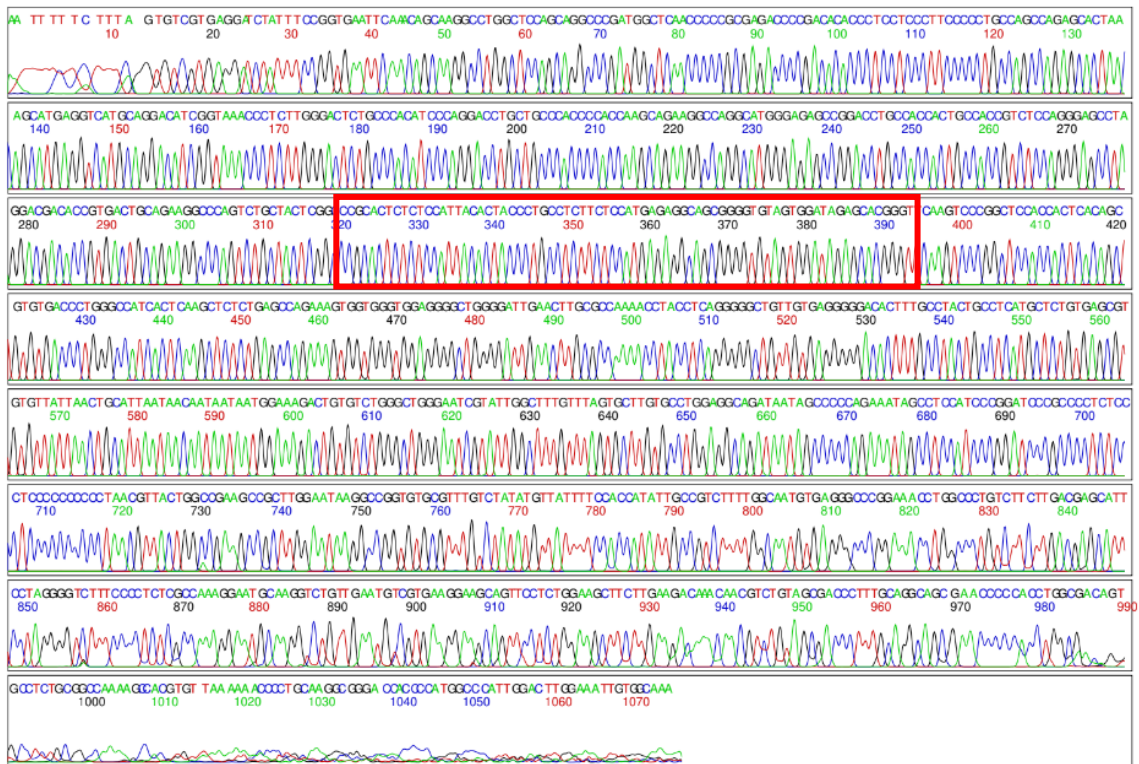
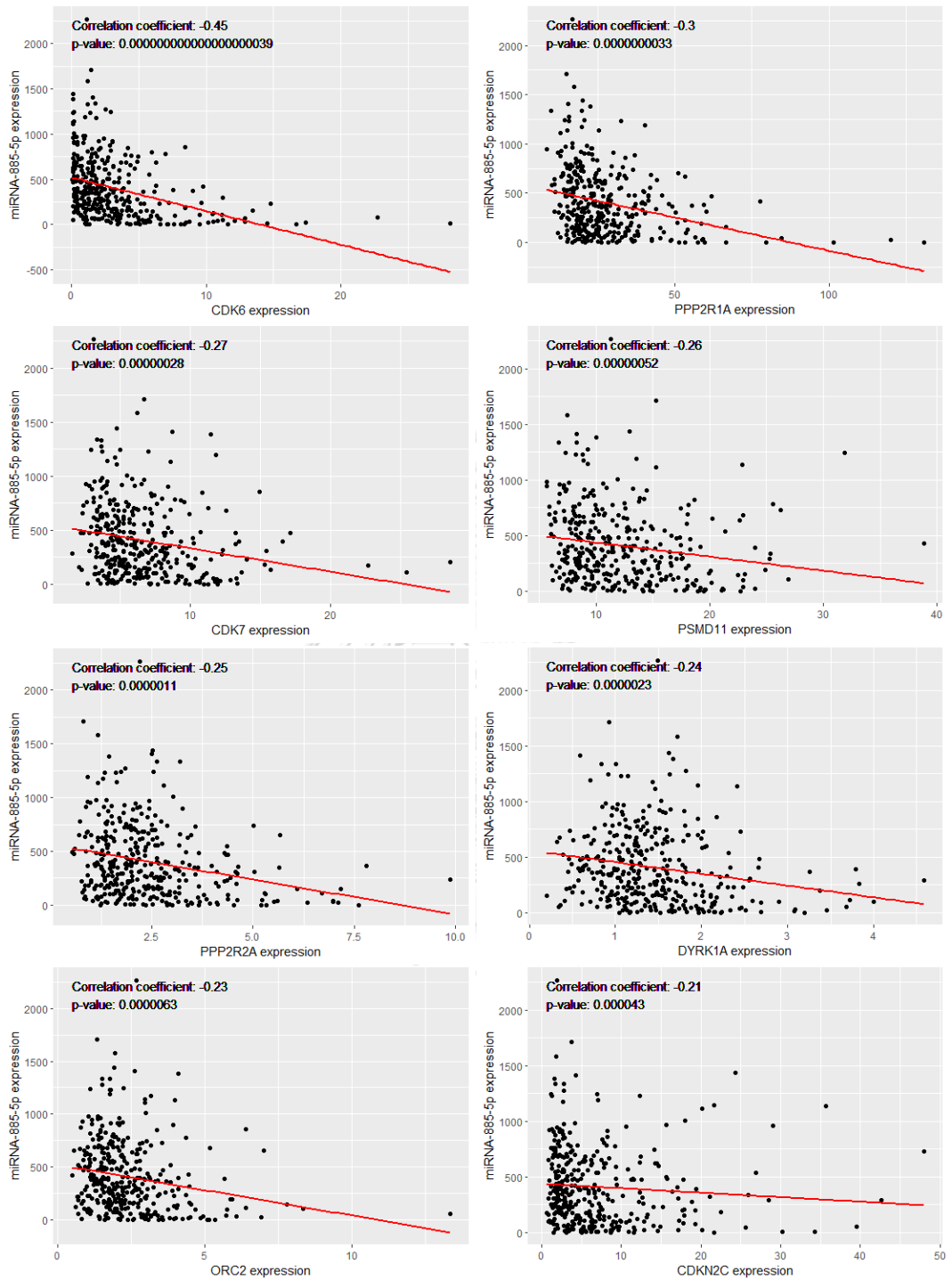
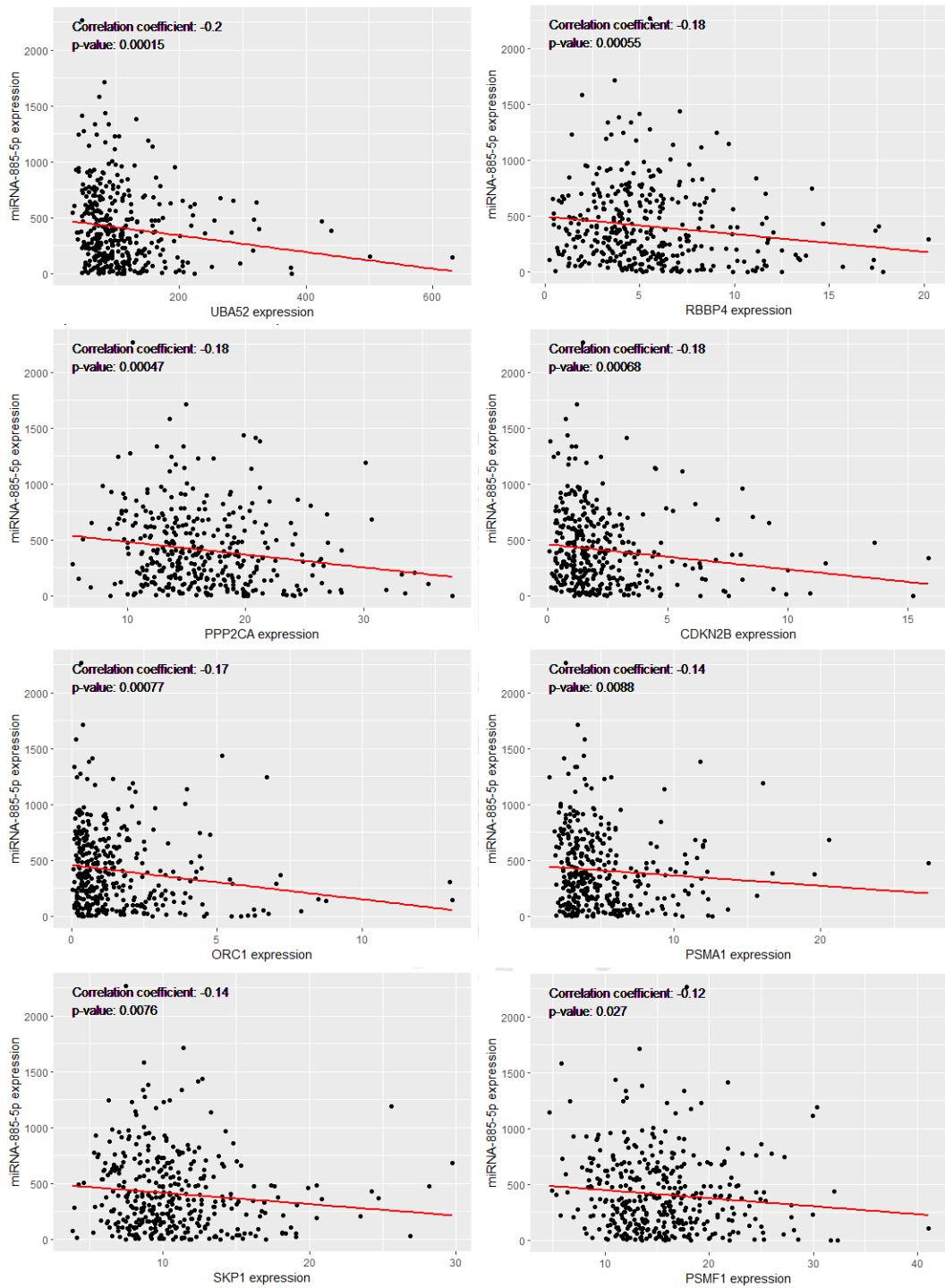


Fig. S2 Sanger sequencing analysis of the pLV-EF1 α -IRES-Puro plasmid containing pri-miRNA of hsa-miR-885. Red box indicates the stem-loop sequence of hsa-miR-885.





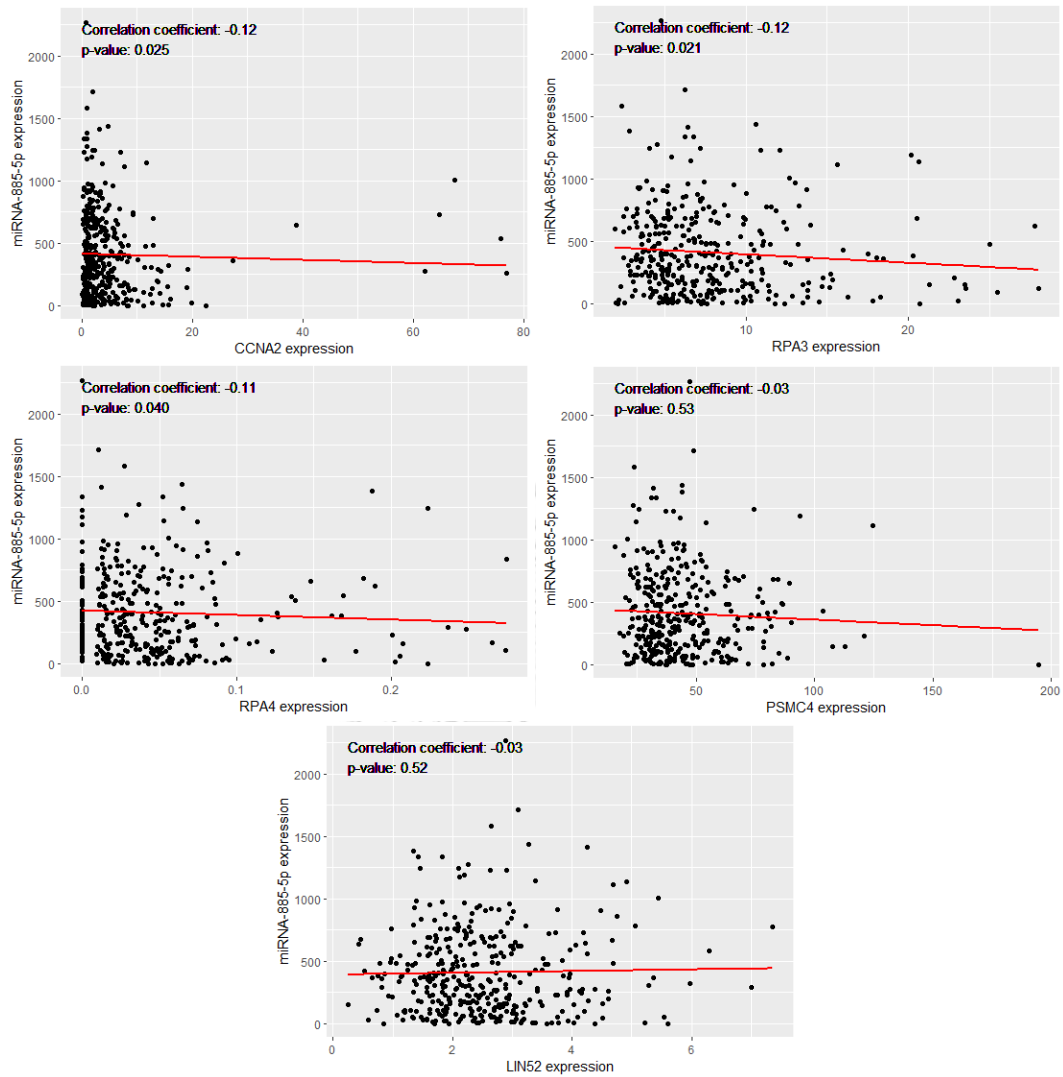


Fig. S3 Correlation analysis of mRNAs and hsa-miR-885-5p.

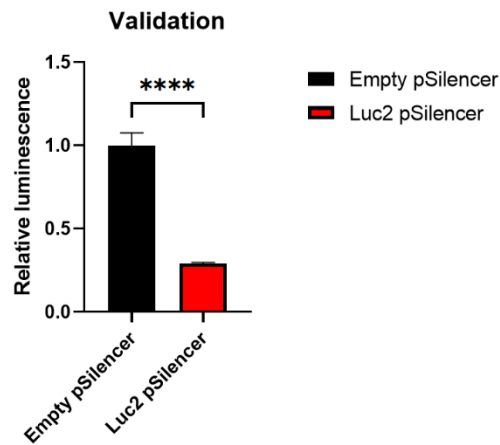


Fig. S4 Validation result of dual-luciferase assay.

REFERENCES



จุฬาลงกรณ์มหาวิทยาลัย
CHULALONGKORN UNIVERSITY

- [1.] Llovet JM, Kelley RK, Villanueva A, Singal AG, Pikarsky E, et al. (2021). Hepatocellular carcinoma. *Nature Reviews Disease Primers*, 7(1), 6.
- [2.] Farazi PA, DePinho RA. (2006). Hepatocellular carcinoma pathogenesis: from genes to environment. *Nature Reviews Cancer*, 6(9), 674-87.
- [3.] Sung H, Ferlay J, Siegel RL, Laversanne M, Soerjomataram I, et al. (2021). Global Cancer Statistics 2020: GLOBOCAN Estimates of Incidence and Mortality Worldwide for 36 Cancers in 185 Countries. *CA: A Cancer Journal for Clinicians*, 71(3), 209-49.
- [4.] Rungay H, Arnold M, Ferlay J, Lesi O, Cabañag CJ, et al. (2022). Global burden of primary liver cancer in 2020 and predictions to 2040. *Journal of Hepatology*, 77(6), 1598-606.
- [5.] Xu G, Jin B, Xian X, Yang H, Zhao H, et al. (2021). Evolutions in the Management of Hepatocellular Carcinoma over Last 4 Decades: An Analysis from the 100 Most Influential Articles in the Field. *Liver Cancer*, 10(2), 137-50.
- [6.] O'Brien J, Hayder H, Zayed Y, Peng C. (2018). Overview of MicroRNA Biogenesis, Mechanisms of Actions, and Circulation. *Frontiers in Endocrinology*, 9.
- [7.] Shrivastava S, Steele R, Ray R, Ray RB. (2015). MicroRNAs: Role in Hepatitis C Virus pathogenesis. *Genes & diseases*, 2(1), 35-45.
- [8.] Xu J, An P, Winkler CA, Yu Y. (2020). Dysregulated microRNAs in Hepatitis B Virus-Related Hepatocellular Carcinoma: Potential as Biomarkers and Therapeutic Targets. *Frontiers in Oncology*, 10.
- [9.] Miranda RC, Pietrzykowski AZ, Tang Y, Sathyan P, Mayfield D, et al. (2010). MicroRNAs: master regulators of ethanol abuse and toxicity? *Alcohol: Clinical and Experimental Research*, 34(4), 575-87.
- [10.] Osterndorff-Kahanek EA, Tiwari GR, Lopez MF, Becker HC, Harris RA, et al. (2018). Long-term ethanol exposure: Temporal pattern of microRNA expression and associated mRNA gene networks in mouse brain. *PLOS ONE*, 13(1), e0190841.
- [11.] Yang W, Lian J, Feng Y, Srinivas S, Guo Z, et al. (2014). Genome-wide miRNA-profiling of aflatoxin B1-induced hepatic injury using deep sequencing. *Toxicology Letters*, 226(2), 140-9.

- [12.] Ferlay J EM, Lam F, Colombet M, Mery L, Piñeros M, Znaor A, Soerjomataram I, Bray F. Global Cancer Observatory: Cancer Today Lyon, France: International Agency for Research on Cancer; 2020 [cited 2023 January 04]. Available from: <https://gco.iarc.fr/today>.
- [13.] Rungay H, Ferlay J, de Martel C, Georges D, Ibrahim AS, et al. (2022). Global, regional and national burden of primary liver cancer by subtype. *European Journal of Cancer*, 161, 108-18.
- [14.] Lyra-González I, Flores-Fong LE, González-García I, Medina-Preciado D, Armendáriz-Borunda J. (2015). MicroRNAs dysregulation in hepatocellular carcinoma: Insights in genomic medicine. *World Journal of Hepatology*, 7(11), 1530-40.
- [15.] Levrero M, Zucman-Rossi J. (2016). Mechanisms of HBV-induced hepatocellular carcinoma. *Journal of Hepatology*, 64(1), S84-S101.
- [16.] Arbuthnot P, Kew M. (2001). Hepatitis B virus and hepatocellular carcinoma. *International Journal of Experimental Pathology*, 82(2), 77-100.
- [17.] Zhang W, He H, Zang M, Wu Q, Zhao H, et al. (2017). Genetic Features of Aflatoxin-Associated Hepatocellular Carcinoma. *Gastroenterology*, 153(1), 249-62.e2.
- [18.] Huang MN, Yu W, Teoh WW, Ardin M, Jusakul A, et al. (2017). Genome-scale mutational signatures of aflatoxin in cells, mice, and human tumors. *Genome Research*, 27(9), 1475-86.
- [19.] M'Bengue AK, Doumbia M, Denoman SR, Ouattara DN, Adoubi I, et al. (2015). A major shift of viral and nutritional risk factors affects the hepatocellular carcinoma risk among Ivorian patients: a preliminary report. *Infectious Agents and Cancer*, 10(1), 18.
- [20.] Liu Y, Wu F. (2010). Global burden of aflatoxin-induced hepatocellular carcinoma: a risk assessment. *Environmental Health Perspectives*, 118(6), 818-24.
- [21.] Samant H, Amiri HS, Zibari GB. (2020). Addressing the worldwide hepatocellular carcinoma: epidemiology, prevention and management. *Journal of Gastrointestinal Oncology*, S361-S73.
- [22.] Suresh D, Srinivas AN, Kumar DP. (2020). Etiology of Hepatocellular Carcinoma: Special Focus on Fatty Liver Disease. *Frontiers in Oncology*, 10.

- [23.] Romano F, Stroppa P, Bravi M, Casotti V, Lucianetti A, et al. (2011). Favorable outcome of primary liver transplantation in children with cirrhosis and hepatocellular carcinoma. *Pediatric Transplantation*, 15(6), 573-9.
- [24.] McGlynn KA, Petrick JL, El-Serag HB. (2021). Epidemiology of Hepatocellular Carcinoma. *Hepatology*, 73 Suppl 1(Suppl 1), 4-13.
- [25.] Leong TYM, Leong ASY. (2005). Epidemiology and carcinogenesis of hepatocellular carcinoma. *HPB*, 7(1), 5-15.
- [26.] Campbell C, Wang T, McNaughton AL, Barnes E, Matthews PC. (2021). Risk factors for the development of hepatocellular carcinoma (HCC) in chronic hepatitis B virus (HBV) infection: a systematic review and meta-analysis. *Journal of Viral Hepatitis*, 28(3), 493-507.
- [27.] Noordeen F. (2015). Hepatitis B virus infection: An insight into infection outcomes and recent treatment options. *Virusdisease*, 26(1-2), 1-8.
- [28.] Tarocchi M, Polvani S, Marroncini G, Galli A. (2014). Molecular mechanism of hepatitis B virus-induced hepatocarcinogenesis. *World Journal of Gastroenterology*, 20(33), 11630-40.
- [29.] Rizzo GEM, Cabibbo G, Craxi A. (2022). Hepatitis B Virus-Associated Hepatocellular Carcinoma. *Viruses*, 14(5), 986.
- [30.] Cha MY, Kim CM, Park YM, Ryu WS. (2004). Hepatitis B virus X protein is essential for the activation of Wnt/beta-catenin signaling in hepatoma cells. *Hepatology*, 39(6), 1683-93.
- [31.] Rawat S, Bouchard MJ. (2015). The hepatitis B virus (HBV) HBx protein activates AKT to simultaneously regulate HBV replication and hepatocyte survival. *Journal of Virology*, 89(2), 999-1012.
- [32.] Moon H, Ro SW. (2021). MAPK/ERK Signaling Pathway in Hepatocellular Carcinoma. *Cancers (Basel)*, 13(12).
- [33.] Yuan K, Lei Y, Chen HN, Chen Y, Zhang T, et al. (2016). HBV-induced ROS accumulation promotes hepatocarcinogenesis through Snail-mediated epigenetic silencing of SOCS3. *Cell Death & Differentiation*, 23(4), 616-27.
- [34.] Elmore LW, Hancock AR, Chang SF, Wang XW, Chang S, et al. (1997). Hepatitis B virus X protein and p53 tumor suppressor interactions in the modulation of

apoptosis. *Proceedings of the National Academy of Sciences of the United States of America*, 94(26), 14707-12.

[35.] Yang JD, Roberts LR. (2010). Hepatocellular carcinoma: a global view. *Nature Reviews Gastroenterology & Hepatology*, 7(8), 448-58.

[36.] Petruzzello A, Marigliano S, Loquercio G, Cozzolino A, Cacciapuoti C. (2016). Global epidemiology of hepatitis C virus infection: An up-date of the distribution and circulation of hepatitis C virus genotypes. *World Journal of Gastroenterology*, 22(34), 7824-40.

[37.] Zhu RX, Seto WK, Lai CL, Yuen MF. (2016). Epidemiology of Hepatocellular Carcinoma in the Asia-Pacific Region. *Gut and Liver*, 10(3), 332-9.

[38.] Basit H TI, Koirala J. *Hepatitis C Treasure Island (FL): StatPearls Publishing*; 2022 Jan [Available from: <https://www.ncbi.nlm.nih.gov/books/NBK430897/>].

[39.] Bandiera S, Billie Bian C, Hoshida Y, Baumert TF, Zeisel MB. (2016). Chronic hepatitis C virus infection and pathogenesis of hepatocellular carcinoma. *Current Opinion in Virology*, 20, 99-105.

[40.] Lingala S, Ghany MG. (2015). Natural History of Hepatitis C. *Gastroenterology Clinics of North America*, 44(4), 717-34.

[41.] El-Serag HB. (2002). Hepatocellular carcinoma and hepatitis C in the United States. *Hepatology*, 36(5 Suppl 1), S74-83.

[42.] Averhoff FM, Glass N, Holtzman D. (2012). Global Burden of Hepatitis C: Considerations for Healthcare Providers in the United States. *Clinical Infectious Diseases*, 55(suppl_1), S10-S5.

[43.] Zampino R, Marrone A, Restivo L, Guerrero B, Sellitto A, et al. (2013). Chronic HCV infection and inflammation: Clinical impact on hepatic and extra-hepatic manifestations. *World Journal of Hepatology*, 5(10), 528-40.

[44.] Vescovo T, Refolo G, Vitagliano G, Fimia GM, Piacentini M. (2016). Molecular mechanisms of hepatitis C virus-induced hepatocellular carcinoma. *Clinical Microbiology and Infection*, 22(10), 853-61.

[45.] Matsushita H, Takaki A. (2019). Alcohol and hepatocellular carcinoma. *BMJ Open Gastroenterology*, 6(1), e000260.

- [46.] Testino G, Leone S, Borro P. (2014). Alcohol and hepatocellular carcinoma: a review and a point of view. *World Journal of Gastroenterology*, 20(43), 15943-54.
- [47.] Ali Samjo S, Abbas Z, Asim M, Tahir K. (2020). The Pattern of Alcohol Consumption and the Severity of Alcohol-related Liver Disease in Patients Visiting the Liver Clinic. *Cureus*, 12(3), e7251.
- [48.] Morgan TR, Mandayam S, Jamal MM. (2004). Alcohol and hepatocellular carcinoma. *Gastroenterology*, 127(5 Suppl 1), S87-96.
- [49.] Taniai M. (2020). Alcohol and hepatocarcinogenesis. *Clinical and Molecular Hepatology*, 26(4), 736-41.
- [50.] Eaton SE, Jagielo-Miller JE, Prendergast MA, Akins CK. (2022). Sex differences in alcohol dehydrogenase levels (ADH) and blood ethanol concentration (BEC) in Japanese quail. *Poultry Science*, 101(5), 101790.
- [51.] Doody EE, Groebner JL, Walker JR, Frizol BM, Tuma DJ, et al. (2017). Ethanol metabolism by alcohol dehydrogenase or cytochrome P(450) 2E1 differentially impairs hepatic protein trafficking and growth hormone signaling. *American journal of physiology. Gastrointestinal and liver physiology*, 313(6), G558-g69.
- [52.] Penaloza CG, Cruz M, Germain G, Jabeen S, Jaydan M, et al. (2020). Higher sensitivity of female cells to ethanol: methylation of DNA lowers Cyp2e1, generating more ROS. *Cell Communication and Signaling*, 18(1), 111.
- [53.] Lu Y, Cederbaum AI. (2008). CYP2E1 and oxidative liver injury by alcohol. *Free Radical Biology and Medicine*, 44(5), 723-38.
- [54.] Mizumoto A, Ohashi S, Hirohashi K, Amanuma Y, Matsuda T, et al. (2017). Molecular Mechanisms of Acetaldehyde-Mediated Carcinogenesis in Squamous Epithelium. *International Journal of Molecular Sciences*, 18(9).
- [55.] Abrar M, Anjum FM, Butt MS, Pasha I, Randhawa MA, et al. (2013). Aflatoxins: biosynthesis, occurrence, toxicity, and remedies. *Critical Reviews in Food Science and Nutrition*, 53(8), 862-74.
- [56.] Saad-Hussein A, Taha MM, Beshir S, Shahy EM, Shaheen W, et al. (2014). Carcinogenic effects of aflatoxin B1 among wheat handlers. *International Journal of Occupational and Environmental Health*, 20(3), 215-9.

- [57.] Hamid AS, Tesfamariam IG, Zhang Y, Zhang ZG. (2013). Aflatoxin B1-induced hepatocellular carcinoma in developing countries: Geographical distribution, mechanism of action and prevention. *Oncology Letters*, 5(4), 1087-92.
- [58.] Ali N. (2019). Aflatoxins in rice: Worldwide occurrence and public health perspectives. *Toxicology Reports*, 6, 1188-97.
- [59.] Pickova D, Ostry V, Toman J, Malir F. (2021). Aflatoxins: History, Significant Milestones, Recent Data on Their Toxicity and Ways to Mitigation. *Toxins*, 13(6), 399.
- [60.] Abrehame S, Manoj VR, Hailu M, Chen Y-Y, Lin Y-C, et al. (2023). Aflatoxins: Source, Detection, Clinical Features and Prevention. *Processes*, 11(1), 204.
- [61.] Macé K, Aguilar F, Wang JS, Vautravers P, Gómez-Lechón M, et al. (1997). Aflatoxin B1-induced DNA adduct formation and p53 mutations in CYP450-expressing human liver cell lines. *Carcinogenesis*, 18(7), 1291-7.
- [62.] Long X-D, Deng Y, Huang X-Y, Yao J-G, Su Q-Y, et al. Molecular Mechanisms of Hepatocellular Carcinoma Related to Aflatoxins: An Update. In: Luis R, editor. *Liver Research and Clinical Management*. Rijeka: IntechOpen; 2017.
- [63.] Guengerich FP, Johnson WW, Shimada T, Ueng Y-F, Yamazaki H, et al. (1998). Activation and detoxication of aflatoxin B1. *Mutation Research/Fundamental and Molecular Mechanisms of Mutagenesis*, 402(1), 121-8.
- [64.] Sohn W, Lee HW, Lee S, Lim JH, Lee MW, et al. (2021). Obesity and the risk of primary liver cancer: A systematic review and meta-analysis. *Clinical and Molecular Hepatology*, 27(1), 157-74.
- [65.] Gupta A, Das A, Majumder K, Arora N, Mayo HG, et al. (2018). Obesity is Independently Associated With Increased Risk of Hepatocellular Cancer-related Mortality: A Systematic Review and Meta-Analysis. *American Journal of Clinical Oncology*, 41(9), 874-81.
- [66.] Marengo A, Rosso C, Bugianesi E. (2016). Liver Cancer: Connections with Obesity, Fatty Liver, and Cirrhosis. *Annual Review of Medicine*, 67(1), 103-17.
- [67.] Fabbrini E, Sullivan S, Klein S. (2010). Obesity and nonalcoholic fatty liver disease: biochemical, metabolic, and clinical implications. *Hepatology*, 51(2), 679-89.
- [68.] Berardo C, Di Pasqua LG, Cagna M, Richelmi P, Vairetti M, et al. (2020). Nonalcoholic Fatty Liver Disease and Non-Alcoholic Steatohepatitis: Current Issues

and Future Perspectives in Preclinical and Clinical Research. *International Journal of Molecular Sciences*, 21(24), 9646.

[69.] Benedict M, Zhang X. (2017). Non-alcoholic fatty liver disease: An expanded review. *World Journal of Hepatology*, 9(16), 715-32.

[70.] Powell EE, Wong VW-S, Rinella M. (2021). Non-alcoholic fatty liver disease. *The Lancet*, 397(10290), 2212-24.

[71.] Schwabe RF, Tabas I, Pajvani UB. (2020). Mechanisms of Fibrosis Development in Nonalcoholic Steatohepatitis. *Gastroenterology*, 158(7), 1913-28.

[72.] Zhai M, Liu Z, Long J, Zhou Q, Yang L, et al. (2021). The incidence trends of liver cirrhosis caused by nonalcoholic steatohepatitis via the GBD study 2017. *Scientific Reports*, 11(1), 5195.

[73.] Karagozian R, Derdák Z, Baffy G. (2014). Obesity-associated mechanisms of hepatocarcinogenesis. *Metabolism*, 63(5), 607-17.

[74.] Suganami T, Tanaka M, Ogawa Y. (2012). Adipose tissue inflammation and ectopic lipid accumulation [Review]. *Endocrine Journal*, 59(10), 849-57.

[75.] Chen H-j, Yan X-y, Sun A, Zhang L, Zhang J, et al. (2023). Adipose extracellular matrix deposition is an indicator of obesity and metabolic disorders. *The Journal of Nutritional Biochemistry*, 111, 109159.

[76.] Lee MJ, Wu Y, Fried SK. (2010). Adipose tissue remodeling in pathophysiology of obesity. *Current Opinion in Clinical Nutrition & Metabolic Care*, 13(4), 371-6.

[77.] Booth A, Magnuson A, Fouts J, Foster M. (2015). Adipose tissue, obesity and adipokines: role in cancer promotion. *Hormone Molecular Biology and Clinical Investigation*, 21(1), 57-74.

[78.] Saeedi P, Petersohn I, Salpea P, Malanda B, Karuranga S, et al. (2019). Global and regional diabetes prevalence estimates for 2019 and projections for 2030 and 2045: Results from the International Diabetes Federation Diabetes Atlas, 9(th) edition. *Diabetes Research and Clinical Practice*, 157, 107843.

[79.] El-Serag HB, Hampel H, Javadi F. (2006). The Association Between Diabetes and Hepatocellular Carcinoma: A Systematic Review of Epidemiologic Evidence. *Clinical Gastroenterology and Hepatology*, 4(3), 369-80.

- [80.] Allaire M, Nault JC. (2016). Type 2 diabetes-associated hepatocellular carcinoma: A molecular profile. *Clinical Liver Disease (Hoboken)*, 8(2), 53-8.
- [81.] El-serag HB, Tran T, Everhart JE. (2004). Diabetes increases the risk of chronic liver disease and hepatocellular carcinoma. *Gastroenterology*, 126(2), 460-8.
- [82.] Fryk E, Olausson J, Mossberg K, Strindberg L, Schmelz M, et al. (2021). Hyperinsulinemia and insulin resistance in the obese may develop as part of a homeostatic response to elevated free fatty acids: A mechanistic case-control and a population-based cohort study. *eBioMedicine*, 65.
- [83.] Landskron G, De la Fuente M, Thuwajit P, Thuwajit C, Hermoso MA. (2014). Chronic inflammation and cytokines in the tumor microenvironment. *Journal of Immunology Research*, 2014, 149185.
- [84.] Chettouh H, Lequoy M, Fartoux L, Vigouroux C, Desbois-Mouthon C. (2015). Hyperinsulinaemia and insulin signalling in the pathogenesis and the clinical course of hepatocellular carcinoma. *Liver International*, 35(10), 2203-17.
- [85.] Raza A, Sood GK. (2014). Hepatocellular carcinoma review: current treatment, and evidence-based medicine. *World Journal of Gastroenterology*, 20(15), 4115-27.
- [86.] Shannon AH, Ruff SM, Pawlik TM. (2022). Expert Insights on Current Treatments for Hepatocellular Carcinoma: Clinical and Molecular Approaches and Bottlenecks to Progress. *Journal of Hepatocellular Carcinoma*, 9, 1247-61.
- [87.] Bartel DP. (2009). MicroRNAs: target recognition and regulatory functions. *Cell*, 136(2), 215-33.
- [88.] Lin S, Gregory RI. (2015). MicroRNA biogenesis pathways in cancer. *Nature Reviews Cancer*, 15(6), 321-33.
- [89.] Szabo G, Bala S. (2013). MicroRNAs in liver disease. *Nature Reviews Gastroenterology & Hepatology*, 10(9), 542-52.
- [90.] Hammond SM. (2015). An overview of microRNAs. *Advanced Drug Delivery Reviews*, 87, 3-14.
- [91.] Fabian MR, Sonenberg N. (2012). The mechanics of miRNA-mediated gene silencing: a look under the hood of miRISC. *Nature Structural & Molecular Biology*, 19(6), 586-93.

- [92.] Winter J, Jung S, Keller S, Gregory RI, Diederichs S. (2009). Many roads to maturity: microRNA biogenesis pathways and their regulation. *Nature Cell Biology*, 11(3), 228-34.
- [93.] Xu X, Tao Y, Shan L, Chen R, Jiang H, et al. (2018). The Role of MicroRNAs in Hepatocellular Carcinoma. *Journal of Cancer*, 9(19), 3557-69.
- [94.] Cimmino A, Calin GA, Fabbri M, Iorio MV, Ferracin M, et al. (2005). miR-15 and miR-16 induce apoptosis by targeting BCL2. *Proceedings of the National Academy of Sciences of the United States of America*, 102(39), 13944-9.
- [95.] Zhang P, Yin J, Yuan L, Wang Q, Du X, et al. (2019). MicroRNA-139 suppresses hepatocellular carcinoma cell proliferation and migration by directly targeting Topoisomerase I. *Oncology Letters*, 17(2), 1903-13.
- [96.] Li Q, Li S, Wu Y, Gao F. (2017). miRNA-708 functions as a tumour suppressor in hepatocellular carcinoma by targeting SMAD3. *Oncology Letters*, 14(2), 2552-8.
- [97.] Liu Z, Sun J, Wang X, Cao Z. (2021). MicroRNA-129-5p promotes proliferation and metastasis of hepatocellular carcinoma by regulating the BMP2 gene. *Experimental and Therapeutic Medicine*, 21(3), 257.
- [98.] Zhuang LK, Yang YT, Ma X, Han B, Wang ZS, et al. (2016). MicroRNA-92b promotes hepatocellular carcinoma progression by targeting Smad7 and is mediated by long non-coding RNA XIST. *Cell Death & Disease*, 7(4), e2203-e.
- [99.] Liao Y, Wang C, Yang Z, Liu W, Yuan Y, et al. (2020). Dysregulated Sp1/miR-130b-3p/HOXA5 axis contributes to tumor angiogenesis and progression of hepatocellular carcinoma. *Theranostics*, 10(12), 5209-24.
- [100.] Inoue J, Inazawa J. (2021). Cancer-associated miRNAs and their therapeutic potential. *Journal of Human Genetics*, 66(9), 937-45.
- [101.] Schafer KA. (1998). The Cell Cycle: A Review. *Veterinary Pathology*, 35(6), 461-78.
- [102.] Ferry I, Kuzan-Fischer CM, Ernoult E, Rutka JT. Chapter 19 - Targeting Cell Cycle Proteins in Brain Cancer. In: Newton HB, editor. *Handbook of Brain Tumor Chemotherapy, Molecular Therapeutics, and Immunotherapy (Second Edition)*: Academic Press; 2018. p. 271-90.

- [103.] Matthews HK, Bertoli C, de Bruin RAM. (2022). Cell cycle control in cancer. *Nature Reviews Molecular Cell Biology*, 23(1), 74-88.
- [104.] Bertoli C, Skotheim JM, de Bruin RA. (2013). Control of cell cycle transcription during G1 and S phases. *Nature Reviews Molecular Cell Biology*, 14(8), 518-28.
- [105.] Wang Z. (2021). Regulation of Cell Cycle Progression by Growth Factor-Induced Cell Signaling. *Cells*, 10(12).
- [106.] Neganova I, Lako M. (2008). G1 to S phase cell cycle transition in somatic and embryonic stem cells. *Journal of Anatomy*, 213(1), 30-44.
- [107.] Barr AR, Cooper S, Heldt FS, Butera F, Stoy H, et al. (2017). DNA damage during S-phase mediates the proliferation-quiescence decision in the subsequent G1 via p21 expression. *Nature Communications*, 8(1), 14728.
- [108.] Malumbres M. (2014). Cyclin-dependent kinases. *Genome Biology*, 15(6), 122.
- [109.] Kim S, Leong A, Kim M, Yang HW. (2022). CDK4/6 initiates Rb inactivation and CDK2 activity coordinates cell-cycle commitment and G1/S transition. *Scientific Reports* 12(1), 16810.
- [110.] Zhang M, Zhang L, Hei R, Li X, Cai H, et al. (2021). CDK inhibitors in cancer therapy, an overview of recent development. *American Journal of Cancer Research*, 11(5), 1913-35.
- [111.] Watt A, Goel S. (2022). Cellular mechanisms underlying response and resistance to CDK4/6 inhibitors in the treatment of hormone receptor-positive breast cancer. *Breast Cancer Research*, 24.
- [112.] Raudvere U, Kolberg L, Kuzmin I, Arak T, Adler P, et al. (2019). g:Profiler: a web server for functional enrichment analysis and conversions of gene lists (2019 update). *Nucleic acids research*, 47.
- [113.] Hua S, Lei L, Deng L, Weng X, Liu C, et al. (2018). miR-139-5p inhibits aerobic glycolysis, cell proliferation, migration, and invasion in hepatocellular carcinoma via a reciprocal regulatory interaction with ETS1. *Oncogene*, 37.
- [114.] Li P, Xiao Z, Luo J, Zhang Y, Lin L. (2019). MiR-139-5p, miR-940 and miR-193a-5p inhibit the growth of hepatocellular carcinoma by targeting SPOCK1. *Journal of Cellular and Molecular Medicine*, 23(4), 2475-88.

- [115.] Liu W, Gao X, Chen X, Zhao N, Sun Y, et al. (2021). miR-139-5p Loss-Mediated WTAP Activation Contributes to Hepatocellular Carcinoma Progression by Promoting the Epithelial to Mesenchymal Transition. *Frontiers in Oncology*, 11.
- [116.] Wong CCL, Wong CM, Tung EKK, Au SLK, Lee JMF, et al. (2011). The MicroRNA miR-139 Suppresses Metastasis and Progression of Hepatocellular Carcinoma by Down-regulating Rho-Kinase 2. *Gastroenterology*, 140(1), 322-31.
- [117.] Wu J, Liu L, Jin H, Li Q, Wang S, et al. (2019). LncSNHG3/miR-139-5p/BMI1 axis regulates proliferation, migration, and invasion in hepatocellular carcinoma. *OncoTargets and Therapy*, 12, 6623-38.
- [118.] Wu J, Zhang T, Chen Y, Ha S. (2020). MiR-139-5p influences hepatocellular carcinoma cell invasion and proliferation capacities via decreasing SLITRK4 expression. *Bioscience Reports*, 40(5).
- [119.] Zan Y, Wang B, Liang L, Deng Y, Tian T, et al. (2019). MicroRNA-139 inhibits hepatocellular carcinoma cell growth through down-regulating karyopherin alpha 2. *Journal of Experimental and Clinical Cancer Research*, 38(1), 182.
- [120.] Zhang Y, Li M, Qiu Y, Wu Y, Chen S, et al. (2022). MiR-139-5p/ENAH Affects Progression of Hepatocellular Carcinoma Cells. *Biochemical Genetics*, 60(6), 2106-19.
- [121.] Zhang Z, Yin J, Yang J, Shen W, Zhang C, et al. (2016). miR-885-5p suppresses hepatocellular carcinoma metastasis and inhibits Wnt/ β -catenin signaling pathway. *Oncotarget*, 7(46), 75038-51.
- [122.] Xu F, Yan J-J, Gan Y, Chang Y, Wang H-L, et al. (2019). miR-885-5p Negatively Regulates Warburg Effect by Silencing Hexokinase 2 in Liver Cancer. *Molecular Therapy - Nucleic Acids*, 18, 308-19.
- [123.] Li C, Wang X, Song Q. (2020). MicroRNA 885-5p Inhibits Hepatocellular Carcinoma Metastasis by Repressing AEG1. *OncoTargets and Therapy*, 13, 981-8.
- [124.] Li D, Liu X, Lin L, Hou J, Li N, et al. (2011). MicroRNA-99a Inhibits Hepatocellular Carcinoma Growth and Correlates with Prognosis of Patients with Hepatocellular Carcinoma*. *Journal of Biological Chemistry*, 286(42), 36677-85.
- [125.] Zhang J, Jin H, Liu H, lv S, Wang B, et al. (2014). MiRNA-99a directly regulates AGO2 through translational repression in hepatocellular carcinoma. *Oncogenesis*, 3(4), e97-e.

- [126.] Zhang J-N, Wei F, Zheng BB, Tang L, Chen F-Y. (2023). Role of miRNA-99a-5p in Modulating the Function of Hepatocellular Carcinoma Cells: Bioinformatics Analysis and *In Vitro* Assay. *Current Cancer Drug Targets*, 23(6), 461-70.
- [127.] Cheng H, Xue J, Yang S, Chen Y, Wang Y, et al. (2017). Co-targeting of IGF1R/mTOR pathway by miR-497 and miR-99a impairs hepatocellular carcinoma development. *Oncotarget*, 8.
- [128.] Kim KH, Sederstrom JM. (2015). Assaying Cell Cycle Status Using Flow Cytometry. *Current Protocols in Molecular Biology*, 111, 28.6.1-6.11.
- [129.] Bracken AP, Ciro M, Cocito A, Helin K. (2004). E2F target genes: unraveling the biology. *Trends in Biochemical Sciences*, 29(8), 409-17.
- [130.] Afanasyeva EA, Mestdagh P, Kumps C, Vandesomepele J, Ehemann V, et al. (2011). MicroRNA miR-885-5p targets CDK2 and MCM5, activates p53 and inhibits proliferation and survival. *Cell Death & Differentiation*, 18(6), 974-84.
- [131.] Jiang Z, Cui H, Zeng S, Li L. (2021). miR-885-5p Inhibits Invasion and Metastasis in Gastric Cancer by Targeting Malic Enzyme 1. *DNA and Cell Biology*, 40(5), 694-705.
- [132.] Liu J, Peng Y, Wei W. (2022). Cell cycle on the crossroad of tumorigenesis and cancer therapy. *Trends in Cell Biology*, 32(1), 30-44.

VITA

NAME Archittapon Nokkeaw

DATE OF BIRTH 10 May 1996

PLACE OF BIRTH Samut Prakan

INSTITUTIONS ATTENDED Chulalongkorn University

HOME ADDRESS 204/21 Phuchao Saming Phray, Samrong Klang, Phra Pradaeng District, Samut Prakan 10130

PUBLICATION Regulatory Functions and Mechanisms of Circular RNAs in Hepatic Stellate Cell Activation and Liver Fibrosis

AWARD RECEIVED Outstanding student



จุฬาลงกรณ์มหาวิทยาลัย
CHULALONGKORN UNIVERSITY